39th AIAA Fluid Dynamics Conference and Exhibit, January 5–8 2009, Orlando FL

Current Status of Basic Research in Hypersonic Turbulence

Alexander J. Smits,*[1] M. Pino Martin†[1] and Sharath Girimaji‡[2]

[1] *Princeton University, Princeton, New Jersey, 08544, United States*

[2] *Texas A & M University, College Station, TX*

The current status of basic research in hypersonic turbulent flows is reviewed. We consider free shear layers, boundary layers, internal flows and shock-wave boundary layer interactions, and discuss experiments as well as computations, including DNS, LES, RANS and RANS-LES hybrid approaches. Important research challenges in external and internal hypersonic flows are identified and some possible future directions are explored. Some recent experimental and computational contributions are summarized.

Nomenclature

$C_h = q_w/\rho_e U_e C_p(T_w - T_r)$ = Stanton number
C_v specific heat at constant volume
C_p specific heat at constant pressure
p pressure, Pa
q_c convective heat transfer rate
q_R radiative heat transfer rate
Re_θ Reynolds number based on momentum thickness
Re_τ friction Reynolds number
u fluctuating component of velocity, m/s
u_τ friction velocity, m/s
U streamwise velocity, m/s
x streamwise distance, m
y normal distance from the wall, m
δ boundary layer thickness, m
ν kinematic viscosity, Pa · s
ρ density, kg/m^3

Superscript
$+$ Indicates inner scaling

Subscript
e Indicates value in the freestream
w Indicates value at wall

Overline indicates time average

*AIAA Fellow
†AIAA Member
‡AIAA Member

I. Introduction

Here, we discuss the current status of basic research in hypersonic turbulent flows. We consider free shear layers, boundary layers, internal flows and shock-wave boundary layer interactions, and we will discuss experiments as well as computations, including DNS, LES and RANS approaches.

To help frame the discussion, it is helpful to consider what we mean when we describe a flow as being hypersonic. According to Anderson,[4] P. L. Roe, in a lecture at the von Kármán Institute, Belgium, in January 1970, commented that

> Almost everyone has their own definition of the term hypersonic. If we were to conduct something like a public opinion poll among those present, and asked everyone to name a Mach number above which the flow of a gas should properly be described as hypersonic there would be a majority of answers round about five or six, but it would be quite possible for someone to advocate, and defend, numbers as small as three, or as high as 12.

Anderson goes on to list some of the distinguishing features of hypersonic flows, including thin shock layers, entropy layers, viscous interactions (essentially displacement effects), high temperature effects, and low density effects (Knudsen number effects). Figure 1 indicates where these effects may become important in the flow over a hypersonic airplane, and a similar figure could be drawn for a re-entry vehicle (which are shaped more like a bluff body), with the added complexity that the gas chemistry may be very different from that of air (Mars, for example, has an atmosphere that is 95% CO_2).

We are concerned only with turbulent flows, and so a number of these distinguishing characteristics are not of primary concern. For example, gas dynamics questions such as the stand-off distance for a shock in a high Mach number flow, a parameter that depends crucially on the gas chemistry, will not be addressed here. Neither will laminar flows, nor transition to turbulence. We will, however, consider high temperature effects, as well as effects originating in the surface conditions such as roughness, ablation, gas injection, and wall cooling. While chemical reactions are not considered, hypersonic internal flow mixing issues including the general effects of heat release will be discussed.

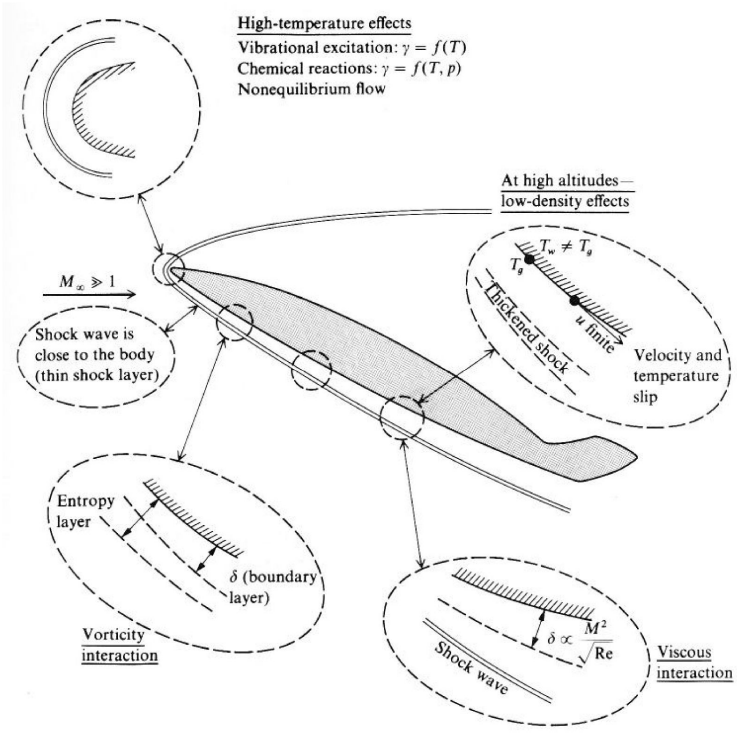

Figure 1. Physical effects characteristic of hypersonic flow.[4]

II. Background

At high Mach number, kinetic energy dissipation by friction in shear layers and by strong shocks create very high temperatures. For air, temperatures in excess of 800K will produce vibrational excitation, and the specific heats C_p and C_v will become functions of temperature, which will reduce the gas temperature below the perfect gas values. At higher temperatures, chemical reactions will occur, and C_p and C_v will become functions of temperature and pressure. Dissociation becomes important for O_2 at about 2000K, and for N_2 above 4000K (at 1 atm), and for temperatures > 9000K, ionization of N and O will become important. This chemistry will be very much more complicated in the case of, say, the Martian atmosphere, and, furthermore, ablation products may be present if an ablative heat shield is used. Strong aerodynamic heating in boundary layers leads to high heat transfer rates to the surface, and this aspect is one of the most important design considerations on hypersonic vehicles and propulsion systems. There are two principal contributions to the surface heat flux: convective heating q_c caused by energy dissipation in the boundary layer due to friction, and radiative heating q_R, which is especially important for important for re-entry configurations. Thermal protection systems (TPS) are a crucial feature of all hypersonic vehicles, well illustrated by the insulating tiles used on the space shuttle and the heat shields used on re-entry vehicles. For sustained operation at high Mach numbers, the wall must be cooled to avoid materials failure. This may be achieved by circulating cooling liquids and gases through the structure supporting the surface itself, or by gas injection. For example, helium is injected into the upstream flow to cool missile and interceptor windows. The gas injection may occur through a slot, where the interaction of the slot jet with the incoming boundary layer is of great interest, or through a porous material, where roughness may become an important factor.

The internal flow Mach number in a hypersonic propulsion device (inlet, isolator, combustor and nozzle) is significantly smaller than the flight Mach number. Nevertheless, along the flow-path the velocity field is subject to various complicating influences such as: compressibility effects (e.g., shock-trains, shock-turbulence and shock-boundary layer interactions), and streamline curvature – in inlet; adverse pressure gradient and separation – in isolator; and mixing and heat release – in combustor. The presence of secondary flows in inlets can profoundly change the mixing (or more accurately, stirring) process. Further, in the combustor, flame-holding strategies seek to increase the residence time for enhancing mixing by introducing recirculation zones into the flow. As is now well recognized, compressibility significantly reduces the mixing efficiency of a turbulent field as quantified by the so-called Langley curve. Thus, compressibility and other effects further exacerbate the already complex flow environment in hypersonic devices. However, our ability to model these phenomena is inadequate due to incomplete understanding of the underlying physical processes.

Within these restrictions, we will now attempt to summarize the current status of research in turbulent hypersonic flows. As we will quickly show, the experimental database for turbulence at Mach numbers greater than 5 is extremely limited. It is also almost exclusively confined to flows of perfect gases, and although it is obvious that this immediately limits the scope of our work, we can only report on progress made in the basic study of turbulence at very high speed and very little can be said on the effects of chemistry on turbulence, except in the simplest of ways.

As to computations, it is clear that considerable progress has already been made in DNS of hypersonic turbulent flows, and the pace of progress is accelerating. Because many high Mach number flow applications are at low Reynolds number, DNS is particularly useful for fundamental studies. Questions of accuracy are being resolved, and with the rapid increase in computer resources even complex shock wave boundary layer interactions can be simulated now or in the near future. In terms of reacting flows, the primary limitations for computations are set by the details of the chemical kinetics, in terms of the number of species and reactions contained in the model, and the uncertainty in the rate constants that need to be specified. This may well prove to be an important limitation in further simulation progress. For production and design codes, turbulence models need to be developed for high Mach number applications. In a later section, we will describe an heirarchical suite of closure models of different degrees of sophistication that may be needed to address the various scientific and technological issues.

III. Experimental Database

Here, we will be concerned with the status of current experimental research on the behavior of turbulent boundary layers at high Mach number. To provide a fuller picture, we will describe some of the general features of the hypersonic turbulent boundary layer, consider some high-quality data sets available on the

surface parameters such as wall pressure, skin friction and heat transfer, as well as the mean flow. With respect to the turbulence itself, we describe all of the past and current efforts to obtain such data, or at least all those known to the present authors.

To illustrate the strong gradients within the hypersonic turbulent boundary layer, Figure 2 shows the data of Watson *et al.*[116] taken in an adiabatic helium flow at Mach 10.3. The temperature is seen to increase by a factor of almost 33 between the freestream and the wall. Note that even at this high Mach number helium behaves as a perfect gas.

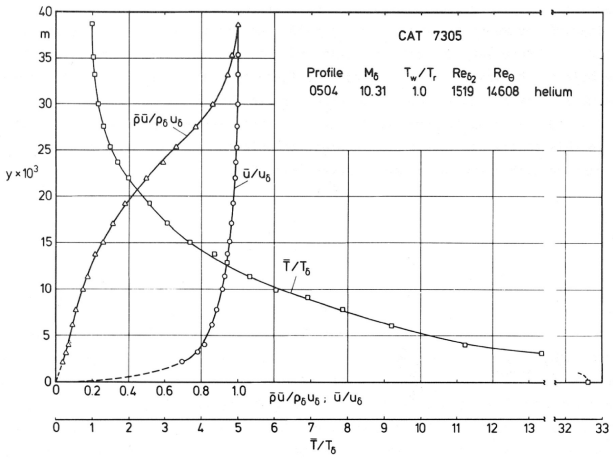

Figure 2. Profiles of temperature, velocity, and mass flow in a Mach 10.3 adiabatic boundary layer flow in helium.[116] Figure taken from Fernholz & Finley.[30]

Figure 2 was taken from AGARDograph 223 authored by Fernholz & Finley.[28] This report was one of a series of AGARDographs that critically assessed the experimental database on supersonic and hypersonic turbulent flows,[28–31] and published the data sets that met their quality standards. In this respect, these efforts did for high speed flows what Coles's Rand report did for incompressible turbulent boundary layer data.[14] These data assessments were extended in 1991 to hypersonic interaction flows by Settles & Dodson,[98] and this collection was updated in 2006 by Roy & Blottner.[91] Perhaps the most surprising aspect of this update was that very few additional experiments had become available in the intervening 15 years.

We will briefly review these experiments, starting with zero pressure gradient turbulent boundary layers, and then moving on to shock-wave boundary layer interactions. In each category, we will first consider surface data (skin friction and heat transfer), then mean flow measurements, and then whatever turbulence data may be available at this time. We will also take the opportunity to compare the data to predictions using relatively standard turbulence models, where possible. This comparison relies heavily on the important work by Roy & Blottner.[91]

A. Zero pressure gradient boundary layers

Figure 3 compares skin friction distributions in zero pressure gradient flows at Mach 8 computed using standard turbulence models and the Van Driest correlation, for flow over a flat plate and flow over a sharp cone. The overall agreement in the fully turbulent part of the flow is within about $\pm 6\%$, which seems rather encouraging except for the fact that no reliable experimental data are available for even these simple flows.

Figure 4 shows a similar comparison for the heat transfer distributions on a sharp cone at Mach 8. The agreement among the different computations in the fully turbulent part of the flow is again within about $\pm 6\%$, and they agree reasonably well with the experimental data where available, although the experiment displays considerable scatter. It would seem that the prediction of heat transfer on a simple cone a this Mach number is probably accurate to within about $\pm 10\%$.

One of the most important experiments in hypersonic turbulent flows was that performed at NASA Ames.[74,77–79] The flow developed on an axisymmetric body, so that it was free of side wall effects, although there may be some residual history effects from the development over the ogive nose body. The upstream boundary layer is representative of a zero pressure gradient Mach 7.2 flow. The mean velocity, shown in Figure 5, follows the standard semi-logarithmic profile when transformed according to Van Driest, which

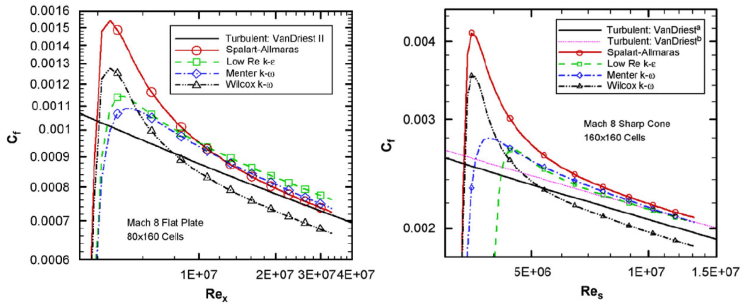

Figure 3. Skin friction distributions in zero pressure gradient flows computed using standard turbulence models and the Van Driest correlation. Left: Flat plate Mach 8 boundary layer flow in air. Right: Sharp cone Mach 8 boundary layer flow in air. Figures taken from Roy & Blottner.[91]

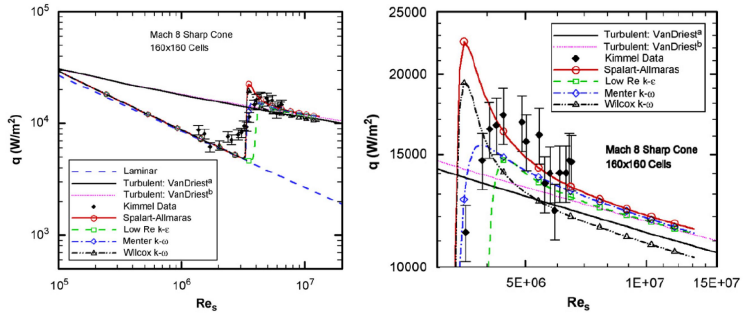

Figure 4. Heat transfer distributions in sharp cone Mach 8 boundary layer flow in air computed using standard turbulence models and the Van Driest correlation. Left: Laminar-turbulent transition. Right: Detailed view of the turbulent regime. Data from Kimmel.[58,59] Figures taken from Roy & Blottner.[91]

takes account of the density changes across the boundary layer. A similar profile, at the same Mach number, was measured by Baumgartner,[7] and support the notion that the scaling laws for the mean flow are essentially independent of Mach number. In addition, McGinley et al. **??** reports data for the mass flux fluctuations obtained using a hot wire in a Mach 11 turbulent boundary layer. These data appear to show the expected level of intermittency in the outer layer, in contrast to the Owen et al. data. Since hot wires measure mass flux intensities and not velocity correlations, deriving the stresses from both sets of measurements requires the use the Strong Reynolds Analogy (see Smits & Dussauge, 2005). Since the validity of the Strong Reynolds Analogy has not been established at hypersonic Mach numbers, the comparison with velocity data are consequently somewhat difficult.

The most important aspect of this experiment, however, is that two-component turbulence measurements were made using hot wire anemometry. These data are, as far as the authors are aware, the only measurements of the turbulent stresses ever made at Mach numbers greater than 5. Some representative results are shown in Figure 6. The figures include data taken downstream of two different reflected shock wave interactions produced by external, axisymmetric shock generators — an attached interaction generated by a 7° wedge, and a separated interaction generated by a 15° wedge.

As to the structure of the turbulence, some very useful information can be obtained by non-intrusive techniques such as Filtered Rayleigh Scattering (FRS). Some visualizations in a vertical slice through the incoming boundary layer using FRS are shown in Figure 7. Regions of cold freestream fluid appear as bright regions, and the regions of turbulent hot fluid appear dark. Deep incursions of freestream fluid can be seen in the near-wall image and turbulent bulges are seen to extend well beyond the mean boundary layer edge in the images taken in the outer layer.

From the FRS images, we can investigate the intermittency, mean structure angles and mean length scales. The intermittency was determined by applying a simple threshold to the grayscale values, and the results are shown in Figure 8. Within experimental error, there is no discernible difference between this supersonic boundary layer and the profile derived for subsonic boundary layers. This result throws some considerable doubt on the accuracy of the hot-wre measurements by Owen *et al.* described earlier, in that

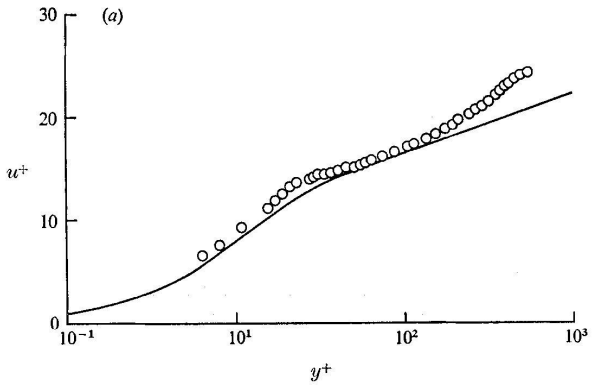

Figure 5. Mean flow measurements in a Mach 7.2 turbulent boundary layer transformed according to Van Driest. Data from Owen *et al.*[79]

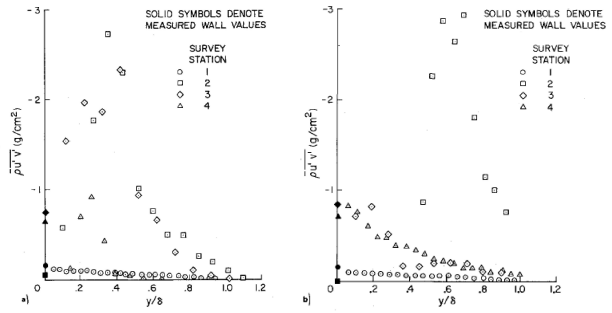

Figure 6. Hot-wire shear stress measurements in a Mach 7.2 reflected shock wave boundary layer interaction. Left: 7° interaction (attached flow). Right: 15° interaction (separated flow). Data from Owen & Horstman[77–79] and Mikulla & Horstman.[74]

their intermittency profile (derived from the flatness data) show a strong MAch number influence which is absent from the data shown here. As to the mean structure angles, the data compare favorably with the hot-wire data of Spina *et al.*[105] ($Ma = 2.9$, $Re_\theta \approx 80,000$), as well as subsonic data.

In brief, the behavior of zero pressure gradient hypersonic turbulent boundary layers appears to follow the subsonic and supersonic data very well. There are still some remaining questions, which include the integral scale behavior, the behavior of the shear stress correlation R_{uv} behavior, the accuracy of the Strong Reynolds Analogy at high Mach number, the growing influence of pressure fluctuations at high Mach number, and the effects of heat transfer on the turbulence itself. These issues are discussed in more detail by Smits & Dussauge,[104] and will not be repeated here, except to point out the sharp decrease in the integral scale with Mach number, shown in Figure 9, which mirrors the Langley curve in many respects.

B. Perturbed boundary layers

In the aerodynamic design of high-speed vehicles, for example, it is necessary to understand and predict with specified accuracy the behavior of turbulence in complex geometries and with complex boundary conditions. It is not surprising therefore that considerable work has been performed to study the effects of perturbations or distortions on the behavior of turbulent boundary layers in high-speed flows, including the effects of pressure gradients, extra strain rates such as streamline curvature, divergence, and dilatation, and the interaction with shock waves. Extensive reviews of this body of work are available.[29–31,101,106] Almost all of the relevant work is experimental in nature, however, because engineering computations cannot provide much insight by themselves, and examples of DNS for perturbed boundary layers in high-speed flow are thus far confined to shock wave-boundary layer interactions.[69,85,117] In this section, we are interested in practical issues such as wall transpiration for cooling or fuel injection, and the associated effects of wall roughness and step changes in heat transfer. To expand the data set available for modeling and code validation, we need to

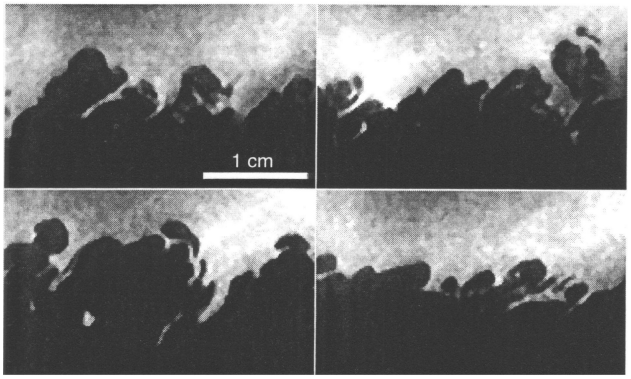

Figure 7. Filtered Rayleigh scattering images of a flat plate boundary layer at Mach 8. Flow is from left to right. The bottom edge of each image corresponds to the plate location. From Bookey *et al.*[9]

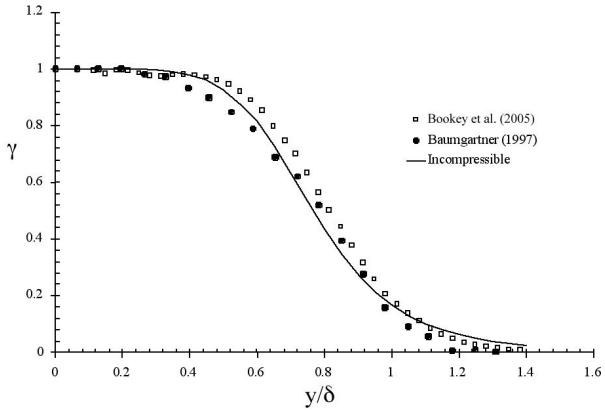

Figure 8. Intermittency profiles deduced from Filtered Rayleigh scattering images of a flat plate boundary layer at Mach 8. From Bookey *et al.*[9]

understand better the effects of gas injection and gas transpiration in transitional and turbulent boundary layers under supersonic and hypersonic conditions.

To illustrate the need for this type of data, previous experiments on perturbed high-speed boundary layers have documented the general features of the mean flow behavior, but there are only a few studies where extensive turbulence measurements have been made (excluding shock-wave boundary layer interactions), most of them quite recently. As indicated by Smits & Dussauge,[104] reliable and accurate turbulence measurements are difficult to make in any supersonic flow, and the difficulties are usually more extreme in the presence of flow distortions and at higher Mach numbers. The questions surrounding the measurements of intermittency using hot wire anemometry in a Mach 7.2 flow has already been discussed. Similarly, many of the experiments that are available were obtained at high Reynolds numbers, and are therefore unsuitable for comparison with DNS. Recent work[9,85,86] has shown conclusively that comparisons between DNS and experiment can only be made at the same Reynolds number: comparing high Reynolds number experiments to low Reynolds number DNS or LES will inevitably lead to incorrect conclusions.

We consider the effects of transpiration from the particular point of view of its effect on the turbulence structure. Recent work by Zhong & Brown[120,121] has given considerable insight on the heat transfer modifications produced by multi-hole cooling of an integrally woven ceramic matrix composite wall. Experiments were performed on the dependence on blowing ratio and the spatial variation in cooling effectiveness, and velocity and temperature profiles were obtained. In Zhong & Brown,[121] DNS calculations of the primary turbulent flow, the backside flow and the flow in the injection holes were coupled by solving the 3-D heat conduction equation for the wall. The cooling effectiveness predicted by the 3-D model was compared with experimental results at the same Reynolds number with a turbulent boundary layer and satisfactory agreement was achieved. Here, we are more concerned with the interaction of the turbulence with transpiration,

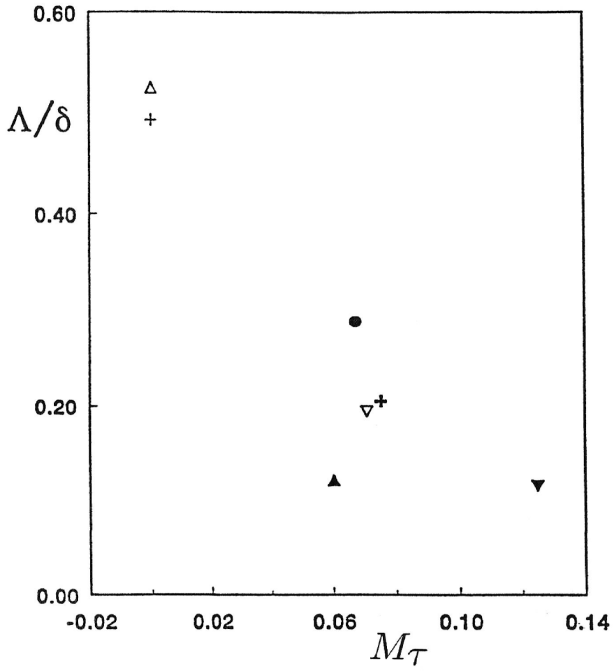

Figure 9. Integral length scale as a function of the friction Mach number ($M_\tau = M_e\sqrt{C_f/2}$). From Dussauge & Smits.[20]

and, as shown by Auvity *et al.*,[5] low momentum sonic helium injection through a transverse slot in a hypersonic boundary layer significantly affects the boundary layer downstream of the injection point, greatly increasing its spanwise organization.

The study was motivated by the suggestion that hydrogen fuel for a hypersonic vehicle could be transpired into the boundary layer upstream of the engine to promote early mixing, which could then be mixed on a larger scale at entry to the engine by the highly vortical nature of the three-dimensional structure of the shock-wave boundary-layer interactions in the inlet. Helium was used in the experiments as a surrogate for hydrogen fuel.

The boundary layer structure was visualized in three orthogonal planes using FRS. Sequential images of the boundary layer were obtained using a MHz imaging system and employed to construct three-dimensional representations of the instantaneous boundary layer behavior. As shown in Figure 10, in the case where helium was injected in a transitional boundary layer, the boundary layer consists of a spanwise succession of crests, characteristic of increased boundary layer thickness, and troughs, characteristic of increased incursions of free-stream fluid. Here J is the ratio of the momentum of the injected flow compared to the freestream flow. The positions of the crests and troughs were found to be stable for injection rates ranging from $J = 0.09$ to $J = 0.15$. It was postulated that this structure was due to the existence of streamwise vortices in the boundary layer created near the injection point.

In the case where helium was injected in a fully turbulent boundary layer, a similar organization of the boundary layer was observed for the same range of J, although it was generally less pronounced. For all conditions considered by Auvity *et al.*,[5] it was shown that pre-existing variations in the boundary layer upstream of the injection slot affected the spanwise structure of the jet by fixing the position of the streamwise organization induced by helium injection. An attempt was made to decrease their influence by using a trip wire but a similar organization of the boundary layer was obtained downstream of the injection slot once the streamwise length of the injection slot was increased from 1 to 3 mm. Another gas, nitrogen, was tested under the same flow and the same injection conditions and no organized structure, as seen with helium injection was revealed.

Current work at Princeton supported by NASA is extending this work to study distributed transpiration (and roughness), using a similar multi-hole insert as tested by Zhong & Brown[120,121] in incompressible flow. The measurement techniques include PIV and thermography. Early progress is reported by.[93] The

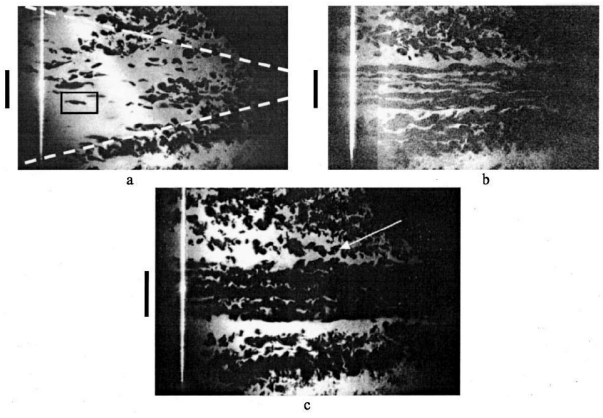

Figure 10. Planform views of the boundary layer at $y = 0.75\delta$ of a Mach 7.2 transitional boundary layer using Filtered Rayleigh Scattering to make density structures visible in a plane: (a) without helium injection; (b) with helium injection, $J = 0.13$; (c) $J = 0.16$. The flow is from left to right, and the slot used for gas injection is shown at left of each image. From Auvity *et al.*[5]

principal objective is to document the change in turbulence structure with increasing levels of roughness and transpiration, and to determine its connection to the changes in heat transfer and surface temperature. The study will include helium injection to investigate whether the strong degree of three-dimensionality observed with slot injection persists in the distributed transpiration regime.

C. Shock wave boundary layer interactions

Our present ability to predict the surface response in hypersonic shock wave boundary layer interactions is well illustrated by the results shown in Figure 11 for the flow in a 34° compression ramp interaction at Mach 9.2. Whereas the pressure distribution is captured with reasonable accuracy, the heat transfer rate within the interaction region is highly unreliable, with the predictions giving values that are from 2 to 5 times higher than those found in the experiments.

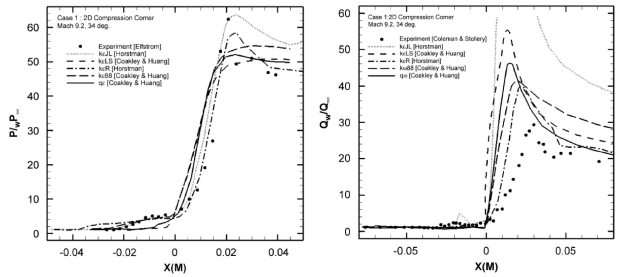

Figure 11. Heat transfer distributions in a 34° compression ramp interaction at Mach 9.2 in air computed using standard turbulence models. Left: Pressure distribution; data from Elfstrom.[26] Right: Heat transfer distribution; data from Coleman & Stollery.[13] Figures taken from Roy & Blottner.[91]

As to the behavior of the turbulence, the experiments by Horstman's group at NASA -Ames on an axisymmetric shock wave boundary layer interaction were described briefly in the previous section (see Figure 6). The strong amplification of the turbulent stresses is clearly evident, with the peak levels exceeding values that are 30 times higher than that seen in the upstream boundary layer. This behavior is as expected, more or less, from similar data taken in supersonic flows,[102] although the accuracy of the hypersonic data is probably somewhat in question.

Bookey *et al.*[9] presented FRS images of an 8° compression ramp shock wave boundary layer interaction at Mach 8, and some representative images are shown in Figure 12. The strong distortion of the shock wave by the turbulence is clearly evident, as is the highly unsteady nature of the interaction.

Bookey *et al.*[9] also studied a 10° sharp fin shock wave boundary layer interaction at Mach 8. The surface

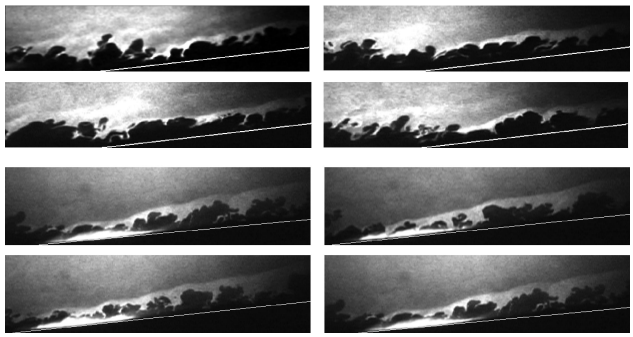

Figure 12. Filtered Rayleigh scattering images of an 8° compression ramp shock wave boundary layer interaction at Mach 8. Top four images are centered on the corner (images are $1.7\delta_0 \times 6\delta_0$), and the bottom four images are taken further downstream (images are $1.8\delta_0 \times 6.5\delta_0$). Flow is from left to right. From Bookey *et al.*[9]

flow visualization of this highly three-dimensional swept shock interaction is shown in Figure 13, and FRS images of the instantaneous turbulence, in two planes normal to the swept shock are shown in Figure 14. The unsteady and turbulent nature of the interaction is obvious, as are the challenges for prediction.

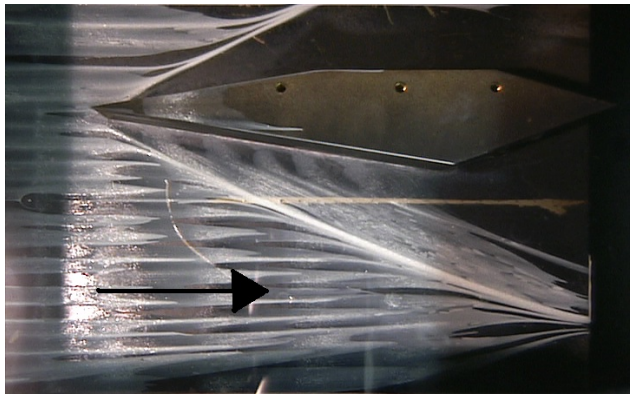

Figure 13. Surface oil flow visualization of a 10° sharp fin shock wave boundary layer interaction at Mach 8. Flow is from left to right. From Bookey *et al.*[9]

There is a decided lack of quantitative data for hypersonic turbulent flows. The evidence shows that the Achilles heel of our understanding is heat transfer. Well-focused experiments and computations, especially direct numerical simulations, are necessary before we can hope to improve our current level of confidence in any predictive scheme. Studies of adiabatic flows are necessary, but for hypersonic flows, adiabatic wall conditions are not representative of flight, where T_w is typically much less than T_r. The usual Reynolds Analogy gives $2C_h/C_f = s$ $(0.9 < s < 1.3)$, but this proportionality breaks down in all perturbed flows, and current models cannot reproduce the observed behavior. The present data base is restricted to ideal gas flows (no chemistry, constant specific heats), and the effects of surface roughness, ablation, chemical reactions, real gases, and body rotation are not adequately addressed by the existing experimental database.

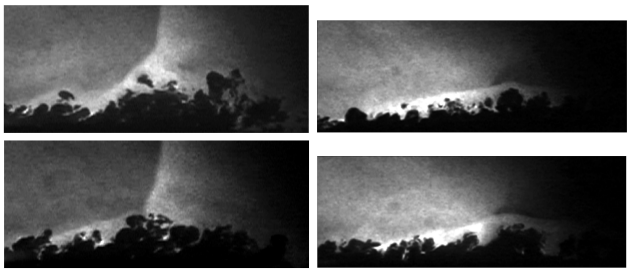

Figure 14. Filtered Rayleigh scattering images of a 10° sharp fin shock wave boundary layer interaction at Mach 8. Left images are at $z = 21$ mm ($\mathbf{1.9}\delta_0$) from the fin (images are $3\delta_0 \times 6\delta_0$). Right images are at $z = 32$ mm ($\mathbf{2.7}\delta_0$) from the fin (images are $2.9\delta_0 \times 7.1\delta_0$). The wall location coincides with the bottom of each image. Flow is from left to right. From Bookey *et al.*[9]

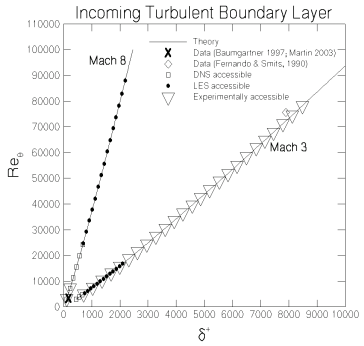

Figure 15. Range of Re_θ and δ^+ for representative boundary layer conditions that are run in the Mach 3 and Mach 8 wind tunnels of the Princeton Forrestal Campus Gas Dynamics Laboratory.

IV. Direct Numerical Simulations

Recent advances in numerical and experimental techniques allow for detailed four-dimensional, in space and time, flow field data acquisition. Direct numerical simulations make possible the computation of turbulent boundary layers at supersonic and hypersonic Mach numbers (Guarini;[47] Martin;[69] Martin;[70] Pirozzoli & Grasso;[80] Xu & Martin;[119] Ringuette, Wu & Martin[87]) as well as the interaction of turbulence with strong, unsteady shock waves (Adams;[1] Pirozzoli & Grasso;[81] Wu & Martin;[117] Wu & Martin;[118] Taylor, Grube & Martin[107]).

The size of the domain and number of grid points required to compute a flow condition can be determined by $\delta^+ = \delta/z_\tau$. Figure 15 plots the Reynolds number based on momentum thickness, Re_θ, for two conditions at Mach 8 and Mach 3. For a given δ^+, Re_θ is significantly larger for the Mach 8 condition. From this perspective, one can argue that δ^+ is a more meaningful parameter to describe the Reynolds number of the flow. Although, one can also argue that accurately measuring the boundary layer thickness is difficult. The Reynolds numbers for hypersonic applications are much lower than those for incompressible flows. If we consider the designed peak heating conditions for Orion NASA crew exploration vehicle earth entry, we find that δ^+ for the attached boundary layer on the capsule is about 360.[75] Performing DNS of the boundary layer for these conditions, including the same chemical mechanism that is being used for design calculations with 13 species, is not a challenge, and we are beginning to introduce radiation physics into the DNS calculations. In the following subsections, we summarize how DNS are being validated and becoming useful to gain insight into the flow physics and to develop phenomenological models and novel turbulence modeling methodologies.

A. Validation of direct numerical simulation data

Studying physical phenomena via joint numerical and experimental databases requires controlled flow conditions. This presents a challenge for numerical simulations, since turbulent flows are highly non-linear and initialization procedures and simulation transients make the final flow conditions difficult to control and costly to obtain if starting from a transitional boundary layer. Martin[70] presented a local initialization procedure that leads to short simulation transients with nearly realistic initial magnitude of turbulence fluctuations, local turbulence structure and energy distribution. This procedure has been applied to initialize turbulent boundary layers over a large range of Reynolds number and Mach numbers, and it has been shown that the procedure leads to controlled flow conditions. The statistical content of the DNS boundary layer data has been validated. Figure 16 presents an example of such validation.

The coherence of the structure in boundary layers is now widely accepted, and it is critical that DNS data produce realistic physics. Theodorsen[109] postulated the existence of the hairpin vortex, a simple flow structure that explains the formation of low-speed streamwise streaks and the ejection of near-wall low-momentum fluid into higher-momentum regions farther from the wall. Head & Bandyopadhyay[49] provided experimental evidence of the streamwise stacking of individual hairpin vortices into larger structures, packets, whose heads describe an envelope inclined at a 15° to 20° downstream angle. More recently, Adrian,

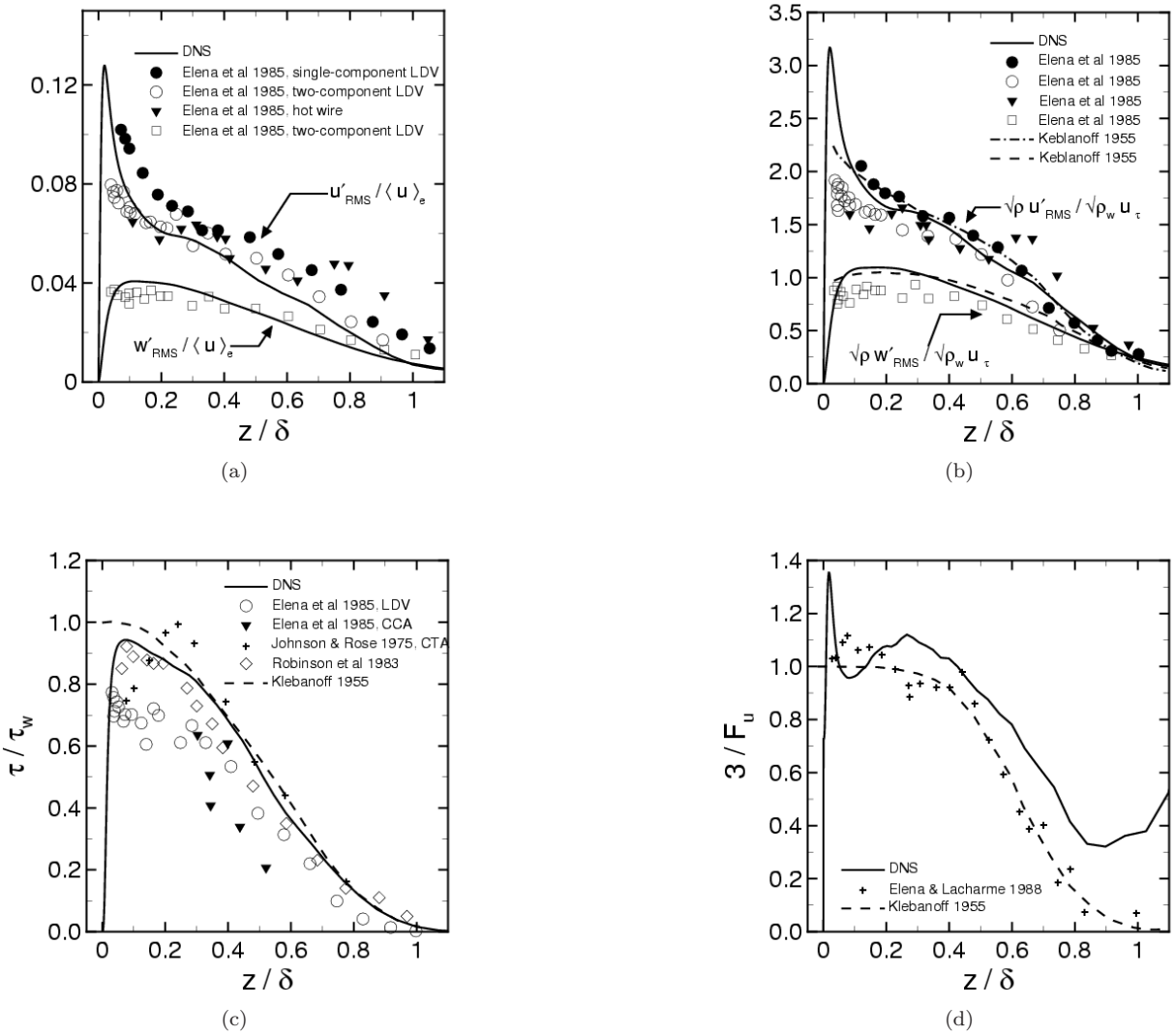

Figure 16. Comparison between DNS at $M = 2.32$ and $Re_\theta = 4450$ and experimental data (Elena *et al.*, 1985; Elena & Lacharme, 1988; Johnson & Rose, 1975; Robinson *et al.*, 1983; Klebanoff, 1955). (a) Magnitude of velocity fluctuations normalized with edge velocity; (b) Magnitude of velocity fluctuations normalized with Morkovin's scaling; (c) Normalized turbulent shear stress; (c) Intermittency factor. From Martin, 2007.

Meinhart, & Tomkins[3] proposed a hairpin packet model, where the hairpins in a packet align in the streamwise direction as observed by Head and Bandyopadhyay. Packets enclose regions of low momentum induced by their heads and counter-rotating legs, and align themselves in the streamwise direction giving rise to the low-momentum, very large-scale motions (VLSM) observed experimentally by Jiménez[54] and Kim & Adrian.[56]

The current study of the turbulence structure in boundary layers has been confined largely to the subsonic flow regime (Tomkins & Adrian;[111] del Álamo & Jiménez;[16] Ganapathisubramani, Longmire & Marusic;[33] del Álamo *et al.*;[17] del Álamo *et al.*;[18] Guala, Hommena & Adrian;[46] Hambleton, Hutchins & Marusic;[48] Flores *et al.*;[32] Balakumar & Adrian;[6] Hutchins & Marusic[51] and Hutchins & Marusic,[52] for example). The study of supersonic and hypersonic turbulent boundary layers has been primarily restricted to statistical analysis, due to the lack of detailed flow field data. Fernholz & Finley;[29] Fernholz & Finley;[30] Spina *et al.*;[106] Smits & Wood;[101] Fernholz;[31] and Smits & Dussauge,[104] give reviews including the effects of pressure gradient, streamline curvature and the interaction with shock waves in high-speed turbulent boundary layers. These descriptions are statistical and some include qualitative flow visualizations. Structure information such as convection velocity, angle, and length scale, has been obtained from space-time correlations (see,

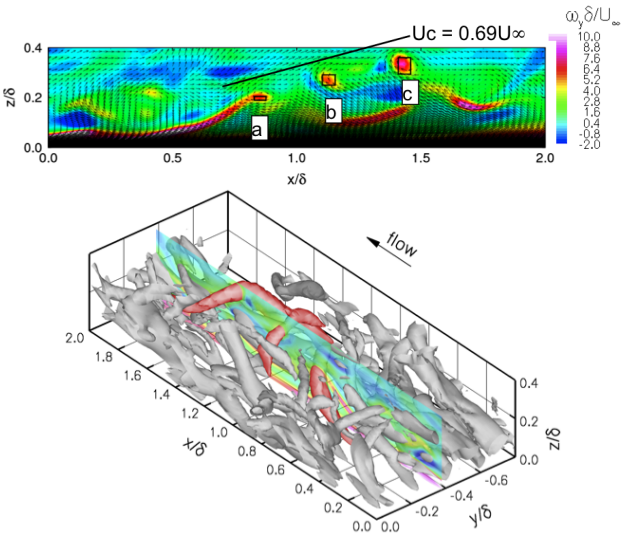

Figure 17. Top: An x-z slice showing a hairpin packet (flow from left to right). Contours show spanwise vorticity and vectors give the in-plane velocity with $0.69U_\delta$ subtracted from u. The black boxes mark the hairpin heads identified by their packet finding algorithm Bottom: The same hairpin packet is visualized in three dimensions using an iso-surface of swirl strength[122] $\lambda_{ci} = 3.5\overline{\lambda_{ci}}$. The $(x,\ z)$-plane data from the top figure are included at 50% translucency for reference. Portions of the packet hairpins not obscured by the reference plane have been colored red. From Ringuette, Wu & Martin 2008.

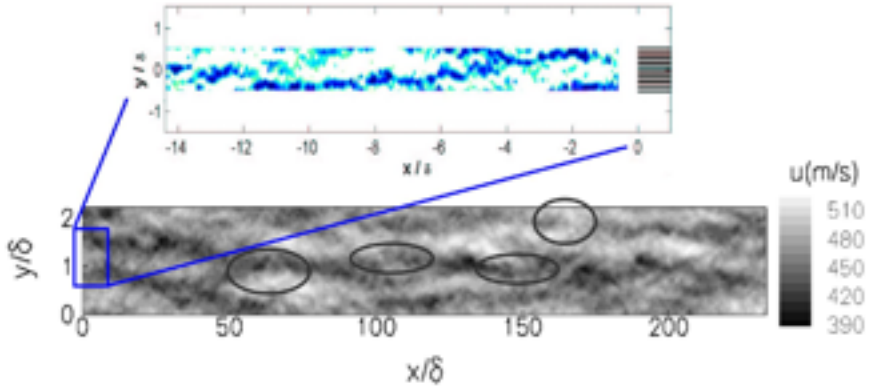

Figure 18. Rake signal from boundary layer data in the logarithmic region visualizing superstructures. Contours of velocity on streamwise-spanwise planes with x-axis reconstruction using Taylor's hypothesis and with convection velocity of about $0.76U_\infty$. Top: atmospheric boundary layer data from Hutchins & Marusic (2007). Bottom: DNS data from Ringuette, Wu & Martin (2008) and Wu & Martin (2008) at Mach 3 adn $Re_\theta = 2300$, with windows showing the location where superstructures begin and end. Data are averaged in $x = 4\delta$ intervals.

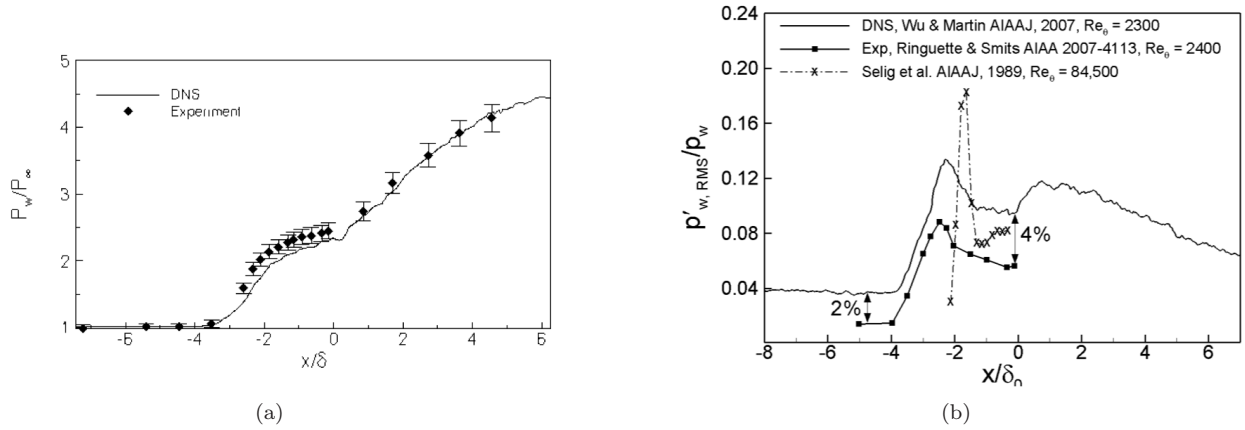

(a) (b)

Figure 19. Validation of DNS data of STBLI against experiemnts for a compression corner interactions with incoming boundary layer at Mach 3 and $Re_\theta = 2400$. (a) Mean wall-pressure distribution from DNS and experimental data. Error bars at 5%. From Wu & Martin (2007). (b) Distributions of $p'_{w,RMS}$ at low and high Reynolds numbers, normalized by the local mean wall pressure, p_w. From Ringuette, Wu & Martin (2008b)

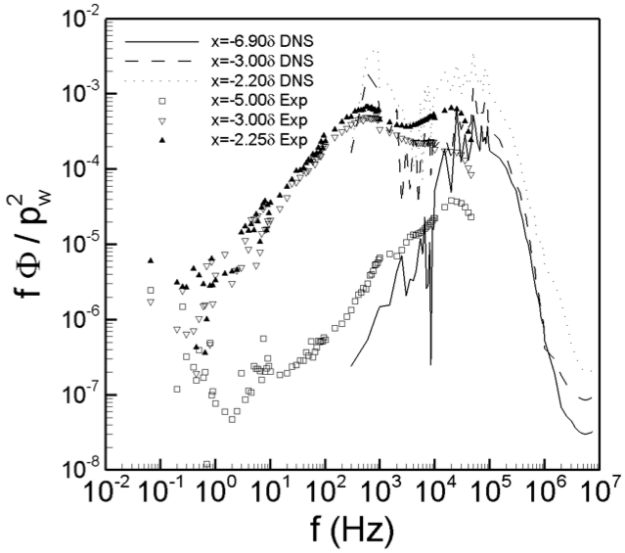

Figure 20. Validation of DNS data of STBLI against experiemnts for a compression corner interactions with incoming boundary layer at Mach 3 and $Re_\theta = 2400$. Pre-multiplied energy spectral density of the wall pressure signal at three different streamwise locations for the DNS (lines) and experiments of Ringuette & Smits (2007) at matching conditions (symbols). The streamwise locations correspond to the incoming boundary layer, the mean separation point, and the peak in the $p'_{w,RMS}$ curve, respectively. From Ringuette, Wu & Martin (2008b).

for example, Smits *et al.*,[103] Spina *et al.*,[105] and Smits & Dussauge[104]). The results indicate changes in structure properties with both Mach and Reynolds numbers, such as a decrease in structure length with increasing Mach number. Advanced particle-image-velocimetry techniques allow the temporal and spatial characterization of experimental supersonic turbulent boundary layers and shock boundary layer interactions (Schrijer, Scarano & van Oudheusden;[113] van Oudheusden;[114] Humble, Scarano & van Oudheusden[115]). Both numerical[87,117] and experimental[34,35] data at supersonic Mach numbers have shown evidence of VLSM. Figures 17 and 18 show the existence of hairpin packets and superstructures in DNS data.

The accuracy of DNS data and its validation against experiments has also been performed in the context of shock and turbulent boundary layer interactions. Adams[1] performed the first DNS for an 18° compression ramp flow at $M = 3$ and $Re_\theta = 1685$. Due to the lack of experimental data at the same flow conditions, at the time, Adams was not able to draw definite conclusions by comparing his DNS with higher Reynolds number experiments.

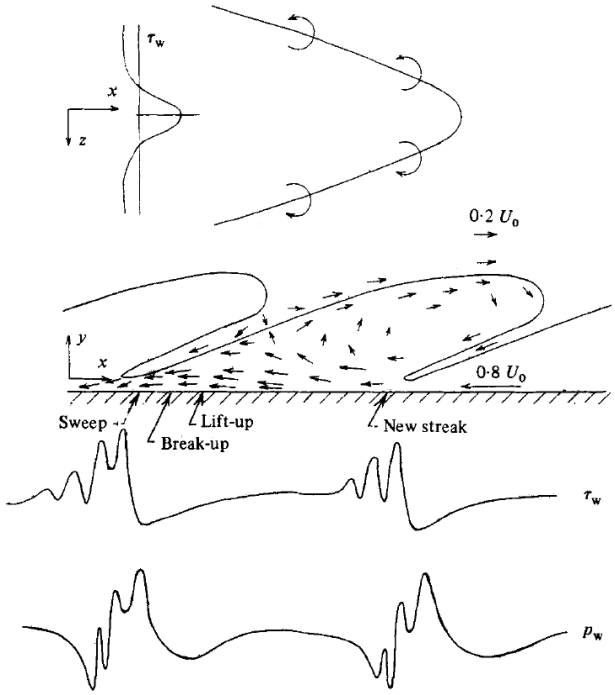

Figure 21. Model of organized structures in turbulent boundary Layers from Thomas & Bull (1983), after Brown & Thomas (1977), as seen by an observer moving at $0.8U_0$.

Pirozzoli and Grasso[81] carried out a DNS of a reflected STBLI at Mach 2.25 and Re_θ 3725 for a deflection angle through the incident shock of 8.1° but experimental data is not available to validate this configuration. Wu & Martin[117] and Ringuette, Wu & Martin[87] perform and validate the DNS of STBLI at Mach 3 and $Re_\theta = 2300$ against the experiments of Bookey et al.[10] and Ringuette & Smits[86] at the same flow and boundary conditions. Figures 19 and 20 plot the validation of the mean, RMS, and frequency content of the wall pressure given by the DNS against the experimental data.

Issues of accuracy and feasibility are being resolved for the configurations described above and we can begin to draw definite conclusions about the effects of Mach number and wall cooling on turbulence and their impact on heat transfer and wall-pressure loading. However, the lack of experimental databases regarding surface transpiration, wall-catalysis, ablation and real gas effects, make it difficult to validate phenomenological scaling relations, even as DNS data becomes available and scalings are proposed.

B. Insight from direct numerical simulation data

We are beginning to draw definite conclusions regarding high Mach number flow physics in turbulent wall-bounded flows, and enabling flow analysis is important to reach that goal. In particular, studying the flow structure can serve to validate statistical interpretations of the data. Brown & Thomas[11] developed a statistical analysis that allows for the calculation of the average inclination angle of packets and to quantify the impact of a passing packet on the wall, i.e. the packet wall signature, which can be measured in terms of pressure or wall-shear stress, see Figure 21. In a recent paper, Beekman *et al.*[8] present a set of analytical tools to study turbulence structures and their wall signature in boundary layers with varying Mach number and wall temperatures. In particular, they use a physically rooted geometric analysis to identify coherent turbulence structures in boundary layer flows, and employ the statistical correlation analysis to validate and interpret the geometrically identified structures and discriminate strong and dynamically dominant structures, while quantifying their impact on the wall pressure loading and heat transfer. Figure 22 plots the average packet velocity given by geometrically identified (strong, average and weak) packets. For reference, the average convection velocity of strong packets given solely by the correlation analysis is also plotted, as well as the mean velocity profile. The data suggest that the average geometric packet is representative of strong statistical packets. Using these tools, Figure 23 shows the automatic tracking of a hairpin packet in DNS data at Mach 3. Figure 24 plots two instantaneous realizations visualizing a hairpin packet in

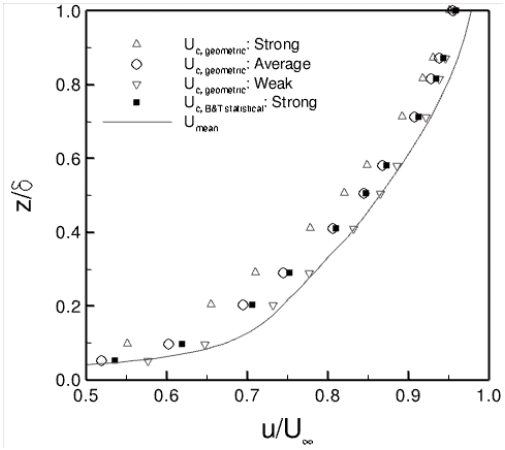

Figure 22. Mach 3 packet convection velocity profiles. The use of the 'geometric events' at the wall limit the statistical correlation analysis to regions where ideal hairpin packets have been found, which correspond to the first three legend entries. The convection velocity determined from the 'strong' Brown and Thomas (1977) correlation is plotted as a square symbol and is quite close in magnitude to the 'average' geometric convection velocity. From Beekman *et al* (2009).

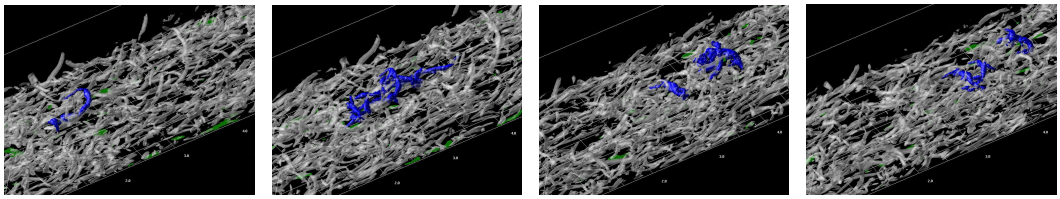

(a) (b) (c) (d)

Figure 23. Tracking hairpin packet in a Mach 3 boundary layer at $Re_\theta = 2,390$. A hairpin packet was identified in 23(a) and highlighted in blue. All other vortices are shown in white and at 50% translucency. The packet was then tracked through subsequent DNS frames. From O'Farrell & Martin (2009) and Beekman *et al.* (2009).

Mach 8 and its wall signature as given by the wall shear stress. The structure of this hairpin packet is cane like, and there is a significant peak in the wall shear stress associated with the tail of the hairpin legs, as hypothesized by Brown & Thomas[11] and Thomas & Bull.[110] Studying the effects of wall temperature and Mach number is being useful in developing a greater understanding of the interaction between turbulence and real gas effects. There are few studies of turbulence-chemistry interaction for hypersonic boundary layers.[66–68] These flows are significantly different from turbulent combustion flows. In hypersonic flows the dominant chemical reactions are the dissociation and recombination of nitrogen or oxygen molecules. The reactions have a high activation energy and the reaction rate is typically temperature limited. In this case, small increases in the temperature result in large increases in reaction rate, which is contrasted with non-premixed combustion flows where the fuel-oxidizer mixing rate determines the rate of product formation and the reaction process is relatively insensitive to the temperature. Martin and Candler[64] study turbulence-chemistry interaction via direct numerical simulation of reacting isotropic turbulence. Their results show that there is a positive feedback between the turbulence and exothermic reactions, and the feedback occurs through the pressure-strain term. Jaberi *et al.*[53] study the turbulence-chemistry interaction in homogeneous decaying compressible turbulence. Their results show that the pressure-dilatation tends to increase the turbulent kinetic energy when the reaction is exothermic. Depending on the flow conditions, the competing effects in boundary layer flows may lead to different turbulence-chemistry interactions, either dominated by exothermicity or by endothermic reactions. In this regard, we are just begining to interpret the DNS data and to report our findings. Duan & Martin[25] find that even when endothermic reactions are dominant in a boundary layer, the heat removal by the reactions can affect the turbulence mixing and enhance the turbulence production terms, see Fig.25. It has been shown that small temperature fluctuations have a significant effect in the chemical composition in boundary layers.[25,67,68] Martin[68] and Martin & Candler[65,67] proposed a scaling for the temperature fluctuations, which in combination with the mean temperature, can

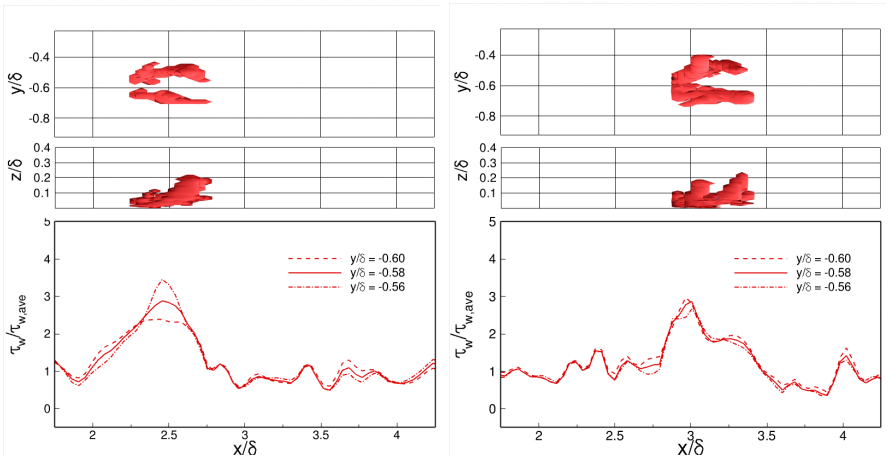

Figure 24. Wall-shear-stress signature of a hairpin packet in DNS of Mach 8 and $Re_\theta = 5100$ boundary layer. The top and middle part of the figure show the packet, visualized by an iso-surface of swirl (the threshold is $4.5\overline{\lambda_{ci}}$). The top part of the figure shows a streamwise-spanwise plane, and the middle part shows a streamwise-wall normal plane. The bottom part of the figure plots the wall-pressure along three different streamwise lines. From Beekman *et al.* (2009). Left and right show two instantaneous realization during the autonomous tracking.

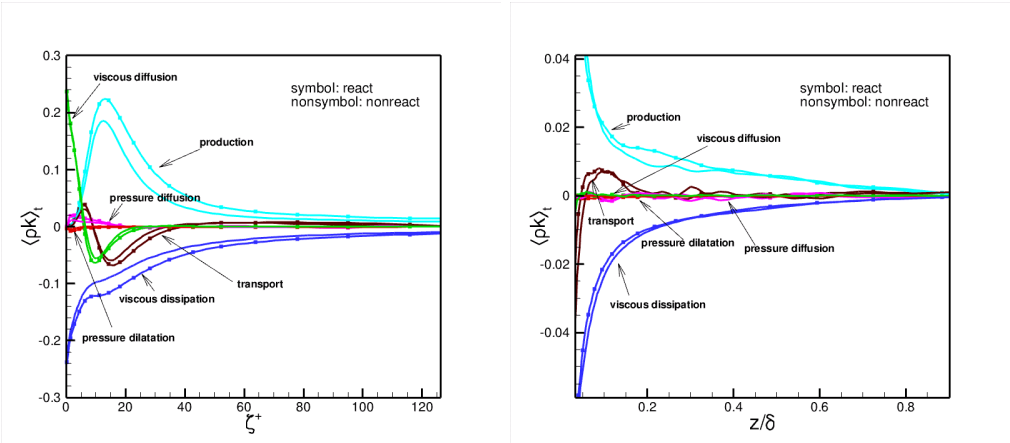

Figure 25. Budget of the terms in the evolution equation for the turbulent kinetic energy from DNS data of a reacting turbulent boundary layer at Mach 4 and $Re_\theta = 3020$. From Duan & Martin (2009).

be used to compute accurate product formation. Yet, there are no experimental data to validate such scaling, although it is currently used to assess the turbulence-chemistry interaction for practical design calculations.

Regarding shockwave and turbulent boundary layer interactions, we still have much to learn about the mechanisms driving the low-frequency interaction, the effects of heat transfer and chemical reactions, and the robust and accurate modeling of such flows for practical applications. . For example, the experimental PIV data of Ganapathisubramani, Clemens & Dolling[35] show that there is a strong correlation between velocity fluctuations in the upstream boundary layer and the separation line surrogate. In contrast, Dussauge *et al.*[21] compile a survey of experimental data covering a range of STBLI configurations and a wide range of Mach and Reynolds number conditions, and they find that the low-frequency of unsteadiness scales with the downstream flow, in terms of the downstream separation length and the freestream velocity. The same scaling also holds for the DNS data in a compression corner[118] and a reflected shock case.[84] We are gathering additional DNS data samples to achieve converged statistics on the upstream and downstream flow correlations. Such analysis will have a significant impact in out ability to understand the mechanisms driving the shock interaction unsteadiness.

In addition, accurate DNS provide a powerful tool to assess and validate modeling methodologies and phenomenological models. For example, Figure 27 plots DNS data of highly compressible isotropic turbu-

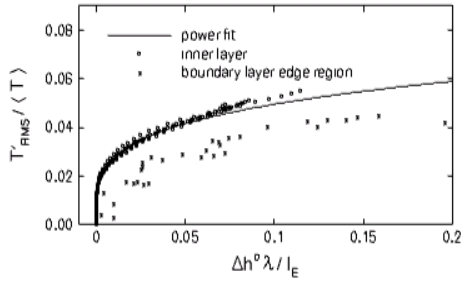

Figure 26. Temperature fluctuation scaling in terms of mean flow variables from DNS data of a reacting boundary layer at Mach 4 and $Re_\theta = 7000$. From Martin & Candler (2001)

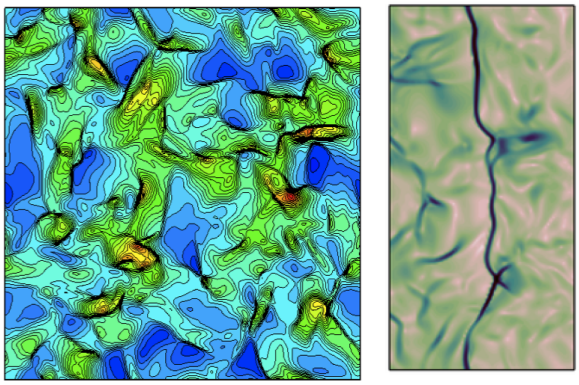

(a) (b)

Figure 27. DNS data of highly compressible isotropic turbulence interacting with shockwaves. (a) Decaying isotropic turbulence at turbulent Mach number ($M_{t\circ}$) of 1.5 and Reynolds ($Re_{\lambda\circ}$) number based on Taylor microscale of 50, density gradients show abundant number of strong shocklets. (b) Contours of normalized density gradient $|\nabla\rho|/\langle\rho\rangle$ on instantaneous cross-section of DNS tested shock/isotropic-turbulence interaction at M=2, $Re_{\lambda\circ} = 35$, $M_{t\circ}$=1,3. From Taylor, Grube & Martin (2007) and Taylor & Martin (2009).

lence. These data are being used to develop robust turbulence modeling of flows involving strong shock waves.[45]

V. RANS-LES Closure-Modeling Suite for internal flows

For the forseeable future the design and development of hypersonic vehicles will depend on computations employing turbulence closure models. In this section, we will discuss the recent developments in hypersonic turbulence closure modeling and computational strategies in the context of internal flows.

Turbulence closure modeling is possible at various degrees of resolution – ranging from fine-grained large eddy simulations (LES) to the coarse-grained Reynolds averaged Navier Stokes (RANS) methods. The resolution and, hence, computational burden is the highest in LES and substantially lesser in RANS. However, the onus on the closure model to accurately represent the physics of unresolved scale is highest in RANS and least in LES: RANS closures are required to capture the physics incumbent in all scales of motion whereas LES models are only called upon to dissipate the right amount of kinetic energy. Consequently, LES computations employ simple algebraic closures and RANS computations may entail solving complex differential equations to bring about the required closure. In general, LES computations are considered to be of higher fidelity but at a very high computational cost with RANS offering more limited accuracy at a very manageable computational effort. Recent times have witnessed the emergence of closure appoaches of intermediate physical accuracy and computational effort. Examples of these variable resolution methods include detached eddy simulations (DES), hybrid RANS-LES and bridging methods such as the Partially Averaged Navier-Stokes (PANS) methods. These methods, based on *accuracy on demand paradigm*, are purported for any degree of resolution between RANS and LES. As in any engineering application, the computational challenges in hypersonic turbulence are to: develop closure models of high-fidelity; and choose the resolution-closure combination to match the physics and fidelity needs. This requires a clear understanding of the flow challenges as well as knowledge of model attributes. In the context of a typical hypersonic propulsion device, we will next describe the various challenges and identify the closure strategy that provides the best balance between computational burden and physical accuracy for each phenomenon.

The complicating physical phenomena encountered along the flow-path of a generic hypersonic device are: shock-trains; shock-boundary layer interactions; fine- and large-scale turbulent mixing; shock/turbulence/ chemistry interactions; pre-mixed and non-premixed reaction zones; and species recombination. The appropriate physics/computation-method combinations are:

1. Intermediate resolution (bridging/hybrid) approach for large-scale shock-induced unsteadiness in inlet and isolator.
2. Fine resolution (perhaps LES) for shock-turbulence interactions and small-scale mixing in fuel-injection zone.
3. Fine resolution for premixed autoignition reaction zone.
4. Intermediate-resolution bridging approach for distributed and non-premixed combustion zones.
5. RANS for far-field and steady reagions of flow-path.

As mentioned earlier, we will not consider chemical kinetics reduction in this paper. Based on the foregoing discussion, we can summarize the objectives of hypersonic turbulence closure modeling research for internal flows as follows:

1. Develop a suite of closure models from RANS to LES to address the range of needs of reacting hypersonic turbulent flows.
2. Integrate the development of closure models at different resolutions and devise strategies to seamlessly blend the computations of different resolutions.
3. Verify and validate individual members of the closure suite in appropriate unit problems.
4. Validate the integrated suit in device size computations.

We will now describe some recent progress toward these goals from research perfomed under NASA NRA and AFOSR funding at Texas A&M University.

A. Outline of integrated model development

One possible strategy for integrated development of closure expressions for various levels of resolution is shown schematically in Fig (28). In the shown approach, closure modeling is performed at the second moment level to take advangate of well-developed turbulence theories and kinematic constraints. Detailed discussions on how rapid distortion theory (RDT), fixed point analysis and realizability constraints can be used to enhance second-moment closures are given in Girimaji *et al.*[39,41,42,92] The equations can be solved at the second moment level, or if needed, they can be reduced to two-equation level using algebraic stress modeling technique.[37,38,40] Finally, the RANS two-equation model can be methodically adapted for bridging (hybrid) method closures. This will be discussed further later. Model development from such an integrated framework will lead to higher fidelity at all levels of closure and easier blending between regions of different resolutions. Now we will identify some of the specific hypersonic turbulence modeling challenges at the RANS level.

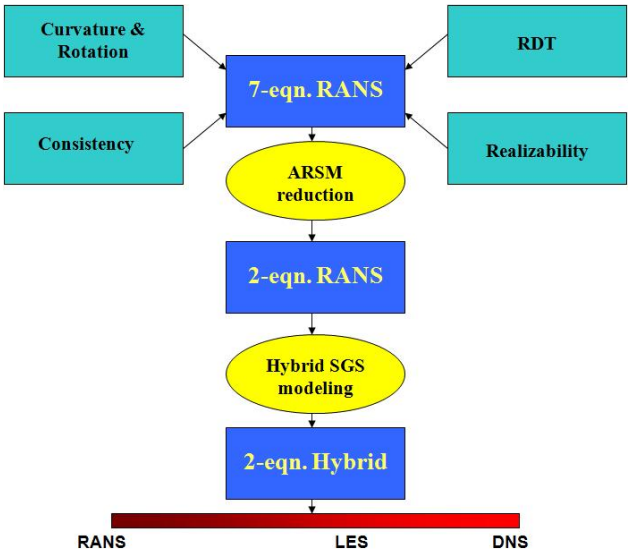

Figure 28. Outline of the integrated model development approach.

In the Favre-averaged conservation equations, the second-order moments – Reynolds shear stress ($\tau_{ij}^T \equiv -\overline{\rho u_i'' u_j''}$), turbulent heat-flux ($q_i^T \equiv \overline{\rho e'' u_i''}$) and species-flux ($J_{ni}^T \equiv \overline{\rho Y_n'' u_i''}$) are the most important unclosed terms. The roadmap for model transport equation development is reasonably well established for compressible flows subject to rapid distortion.[2] We will start this discussion with the Reynolds stress transport equation in a multi-species mixture:

$$\begin{aligned}\tau_{ij,t}^T + \left(\tilde{u}_k \tau_{ij}^T\right)_{,k} = &-\tau_{ik}^T \tilde{u}_{j,k} - \tau_{jk}^T \tilde{u}_{i,k} - \overline{u_j''}\left(-\tilde{p}_{,j} + \tilde{\tau}_{jk,k}\right) + \left(\overline{p_{,i}'' u_j''}\right) + \left(\overline{p_{,j}'' u_i''}\right) \\ &- \sum_n \left[f_{b(n)i}\overline{\rho u_j'' Y_{(n)}''} + f_{b(n)j}\overline{\rho u_i'' Y_{(n)}''}\right] \\ &+ \left[\overline{\left(\rho u_i'' u_j'' u_k''\right)} + \overline{\left(\tau_{ik}'' u_j'' + \tau_{jk}'' u_i''\right)}\right]_{,k} + \overline{\tau_{ik}'' u_{j,k}'' + \tau_{jk}'' u_{i,k}''}\end{aligned}$$

For ease of discussion we will rewrite the Reynolds stress transport equation symbolically as:

$$\tau_{ij,t}^T + \left(\overline{u}_k \tau_{ij}^T\right)_{,k} = P_{ij} + \Pi_{ij} - \epsilon_{ij} + T_{ij} + B_{ij}$$

The terms on the right hand side are production, pressure-strain correlation, dissipation, turbulent diffusion and body-force effect (if present). The transport equations of turbulent heat-flux and species-flux are similar in form. Let **F**, generically referred to as scalar flux ($F_j \equiv \overline{\rho \phi^* u_j''}$) represent either turbulent heat flux **q** or turbulent species flux **J**. The species sub-script is omitted for convenience. The generic scalar flux evolution

equation can be derived from the fluctuating mass (or energy) and momentum conservation equations:

$$\frac{\partial\overline{\rho\phi^* u_j^{''}}}{\partial t} + \frac{\partial\tilde{u}_k\overline{\rho\phi^* u_j^{''}}}{\partial x_k} = \overline{\rho\phi^* u_k^{''}}\frac{\partial\tilde{u}_j}{\partial x_k} + \overline{\rho u_j^{''} u_k^{''}}\frac{\partial\Phi}{\partial x_k} + \overline{p\frac{\partial\phi^*}{\partial x_j}} + \overline{\dot{\omega}^{''} u_j^{''}} + T_{ij} - \epsilon_j + C_j$$

In above equation, the first two terms on the RHS constitute the production of scalar flux; the third term represents the pressure-scalar gradient correlation; fourth term represents the chemical source of flux; T_j, D_j, and C_j are transport, destruction-type and compressibility-related terms respectively. For ease of further discussion, we will again write this equation symbolically as

$$F_{i,t} + \left(\overline{u}_k F_i\right)_{,k} = P_i + \Pi_i - \epsilon_i + T_i + S_i$$

where the various terms in the right hand side are scalar-flux production, pressure-correlation, dissipation and turbulent transport /diffusion and chemical source term. The chemical source term in species equation is due chemical conversion and in the temperature equation is due to heat release/absorption.

Key unclosed terms that need to be modeled in Reynolds stress and flux equations can be generically identified as: pressure correlations, dissipation, turbulent diffusion and chemical source term. While most of the following discussion may in the context of Reynolds stress modeling, all of the arguments are equally applicable for scalar and temperature fluxes as well.

1. *Pressure correlations.* The pressure correlations can be subdivided into rapid and slow pressure correlations. Much of the velocity field linear stability physics is incumbent in the rapid-pressure correlation term. By making the rapid pressure-strain correlation closure consistent with rapid distortion theory (RDT), some multi-point physics can be incorporated into the Reynolds stress model. To inculcate compressibility physics, the rapid model must be made consistent with compressible RDT. The current rapid models are only consistent with incompressible RDT (e.g., *via* Crow constraint), but not compressible RDT. In recent work, we have demonstrated that the current models fail drastically when the flow is compressible as the wave nature of pressure is not accurately replicated in incompressible models. Indeed, the stabilizing physics of compressibility (as quantified in Langley curve) must come from the rapid pressure term.[95] The behavior of slow-pressure terms need further investigation, but they may not play a key role. Some preliminary results indicate that the dilatational components may return to isotropy at acoustic timescale. In contrast, the return to isotropy of solenoidal fluctuations proceeds at turbulence timescale.

2. *Dissipation*: For near-wall flows, it has been found that turbulence frequency equation is a better choice than the dissipation equation. It is currently held belief that dilatational dissipation will not make an important contribution. However, the source (production) term in the dissipation equation may have to be modified to include pressure-dilatation energy transfer.

3. *Turbulent diffusion of stress and fluxes*: While gradient diffusion models have served us well, more needs to be done. There may not be specific hypersonics related issues in this term but further investigations are necessary.

4. *Chemical source term*: In scalar and heat flux equations, there will be a chemical source term due to reactions. Modeling of this term as equally challenging in incompressible flows as in compressible flows. As mentioned in the Introduction, we will not address this issue.

B. Pressure-strain closure modeling of compressibility effects

It has been shown in previous works[12,95] that rapid pressure-strain correlation plays a key role toward reducing turbulent mixing in high-speed flows. Consequently, accurate closure modeling of rapid pressure-strain correlation is vital for precise prediction of hypersonic flows. The best approach to incorporating the correct rapid-pressure physics into closure models is to make them consistent with RDT at hypersonic Mach numbers. In Figure 29, we show RDT calculations of kinetic energy evolution in a homogeneous shear flow as a function of gradient Mach number. It is evident from the figure that at intermediate gradient Mach numbers (1-6) the turbulent kinetic energy grows significantly slowly compared to the incompressible case. However, at much higher Mach numbers, the kinetic energy grows more rapidly than at incompressible Mach numbers. To explain the observed behavior, a recently concluded study suggest the existence of three Mach number regimes of distinctly different pressure-strain correlation behavior.[62] In the *low Mach number regime*, the pressure-field is governed by the Poisson equation and the incompressible models describe the physics adequately. In the *high Mach number regime*, the pressure effect is negligible rendering pressure-strain correlation nearly zero. This permits efficient production of kinetic energy without the disruptive

redistributive pressure-strain correlation effects experienced in incompressible flows. The physics in the *intermediate Mach number regime* is quite different from either limiting case. Pressure evolves according to wave equation and its effect is to block production. This leads to significant reduction in kinetic energy growth. In summary, while important progress has been made in pressure-strain correlation modeling of hypersonic flows, much more research is needed to develop high fidelity computational tools.

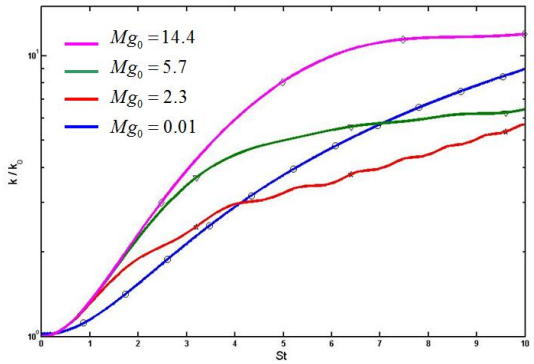

Figure 29. RDT homogeneous shear kinetic energy growth at various Mach numbers.

C. Variable viscosity/diffusivity effects on mechanical/scalar dissipation

One of the key features of hypersonic flows is that the fluid viscosity, diffusivity and other transport properties vary significantly in space and time due to viscous heating and chemical reactions. This raises a very important question: How is Taylor's postulate that dissipation is independent of viscosity affected by strong spatial and temporal variations in viscosity? This postulate is central to much closure model development. The validity of the postulate itself depends on the delicate balance between the inviscid generation of dissipation and its viscous destruction. Invalidity of this postulate will entail the complete revamping of the dissipation model equation in hypersonic flows. Such a total overhaul of the tried and tested equation can be a very challenging task. Recently, it has been shown that this postulate is indeed valid even when viscosity varies by a factor of five in a flow field.[63]

On the scalar mixing side, the equivalent postulate is that scalar dissipation (which is a key mixing feature) is independent of diffusivity. To verify the validity of this postulate, we perfom a 256^3 decaying turbulence DNS study similar to that done by Lee *et al.*[63] The velocity field is initially homogeneous and isotropic with a Taylor-scale Reynolds number of about 200. Two initially-segregated passive scalar fields of identical density but diffusivity different by a factor five are resident in the velocity field as shown in Figure 30. The low-diffusivity fluid occupies one half of the computational box and the high-diffusivity fluid is resident in the other. Due to the nature of the initial conditions, the scalar dissipation in the two halves is different by a factor of five. With passage of time the scalar fields mix in the decaying turbulent velocity field. The spatial variation of plane-averaged diffusivity and scalar dissipation are shown in Figure 31 at various times. The figure shows that within one-half eddy turn-over time, the scalar dissipation is nearly uniform throughout the flow field, eventhough the diffusivity itself is a strong function of space. In Figure 32, we show contours of scalar gradient magnitude and scalar dissipation at three different times. The contour plots show that the scalar grdients become progressively weak in the high viscosity side when compared to the low viscosity side. Yet, in keeping with Taylor's postulate, the product of scalar-gradient squared and diffusivity is constant across the flow field. The results clearly indicate that scalar equivalent of Taylor's postulate is valid even in the presence of strong diffusivity variations. This finding is crucial for closure modeling hypersonic mixing phenomena.

D. Preliminary PANS bridging method results

While high-fidelity RANS may be quite adequate for many parts of the internal flow path, there will be regions of flow, e.g., flame holding area, where unsteady effects and large scale coherent structures play a dominant role. Moreover, the level of accuracy required in these regions may be higher as precise description

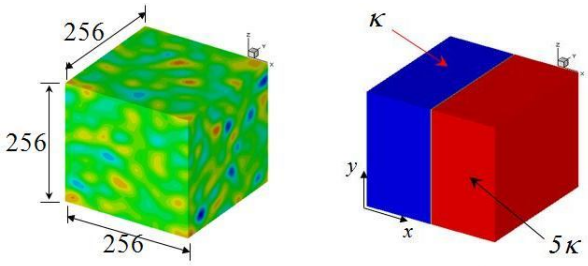

Figure 30. Initial conditions of velocity (left) and diffusivity field (right) in variable diffusivity study. Wavenumber $\kappa = 1$ to 16, $Re_\lambda = 200$.

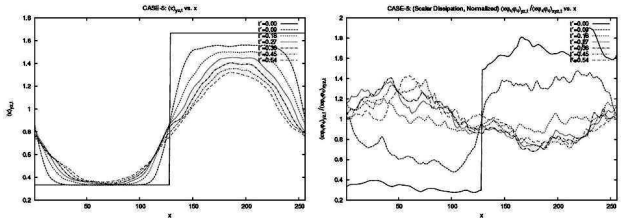

Figure 31. Line plots of diffusivity (left) and scalar gradient (right) as a function of space at different times. Various times (normalized by eddy-turn-over time) are: 0.0, 0.09, 0.18, 0.27, 0.36 and 0.45. Initial condition in both cases is a step function. Scalar dissipation smooths out very quickly validating Taylor's postulate for scalar fields.

of mixing, entrainment of air into the fuel stream and other phenomena that precede chemical reaction is required. As a rule of thumb, accurate prediction of mixing requires a more precise description of velocity field than needed for accurate calculation of aerodynamic quantities such as drag, lift etc. This is because turbulent mixing involves all scales of motion, not just mean flow or the largest scales only. Imprecise modeling of mixing can lead to very poor calculations of chemical reactions and heat release. For turbulent mixing regions with inherent unsteadiness and large coherent structures, even the best RANS models (or any one-point closure) are inherently inadequate and unreliable. Hybrid or bridging models such as the Partially-Averaged Navier-Stokes (PANS) may be more appropriate.[43,44,61] The most important capability of PANS is that it can compute a flow at different cut-off widths controlled by the fraction of unresolved kinetic energy f_k. This fraction must be in commensurate with computational resolution and the exact relationship between the two can be found in the above literature.

Many flow internal and external flow computations using PANS can be found in literature listed above. Here we will consider two preliminary computations of relevance to flame holding: 3-D driven cavity flow and transverse diamond-jet injection into supersonic free stream at Mach number 5. In Figure 33 we compare RANS and PANS calculations against experimental data for the case of 3-D driven cavity flow. These simulations are performed using the commercial code FLUENT employing user defined functions (UDFs). The mean stream-wise velocity at the symmetry plane is plotted as a function of cavity height. RANS model produces reasonably good agreement although PANS predictions are much more accurate. It may appear that RANS is adequate for engineering computations. However, to probe further, we present RANS and PANS flow field vorticity iso-contours in Figure 34. This figure paints a completely different picture. The small scale vortical structure that is crucial for scalar mixing is absent in the RANS computation. It is clear that the mixing characteristics of unsteady RANS and PANS are completely different. For an accurate account of mixing and flame-holding it is imperative that we resolve more scales of motion than RANS. Our second sample calculation involves a cross flow jet exiting normally at Mach 1 from a diamond shaped orifice into a Mach 5 freestream. The DES and PANS simulations are performed using the Cobalt flow solver with PANS modifications added by James Forsythe at Cobalt Solutions, LLC. To compare the closure modeling physics of DES against PANS, the DES and PANS ($f_k = 0.35$) simulations are performed on the same grid. A freestream boundary layer was specified at the inlet to match experimental conditions. No symmetry planes were used to accommodate asymmetries in the flow domain. The injector port was also modeled to account for losses. The total number of cells (hexahedrons) was approximately 10 million. The

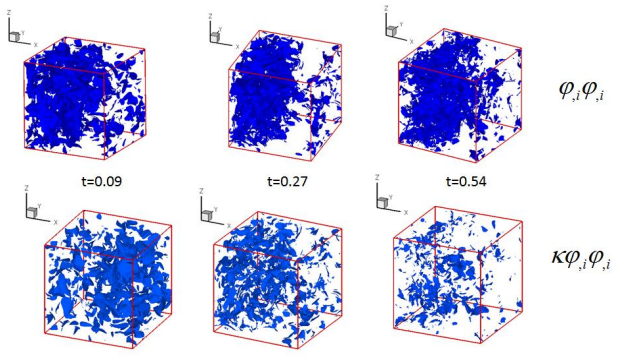

Figure 32. Contour plots of velocity gradients and dissipation at various times. Scalar gradients show sharp spatial variations whereas the scalar dissipation is more uniform.

results from the DES and PANS ($f_k = 0.35$ and 0.2) simulations are shown in Figure 35. The freestream flow is from bottom left to top right. The images represent iso-surfaces of entropy at an identical scale. The iso-surface is colored by temperature. The results show that the flow exhibits more structures when the model is switched from DES to PANS ($f_k = 0.35$). At $f_k = 0.20$, even more structures are seen including the shear layer vortices. The PANS results at Mach 5 and Mach 2 (results not shown) agree well qualitatively with published experimental data. The importance of accurate bridging models are clearly evident from this study.

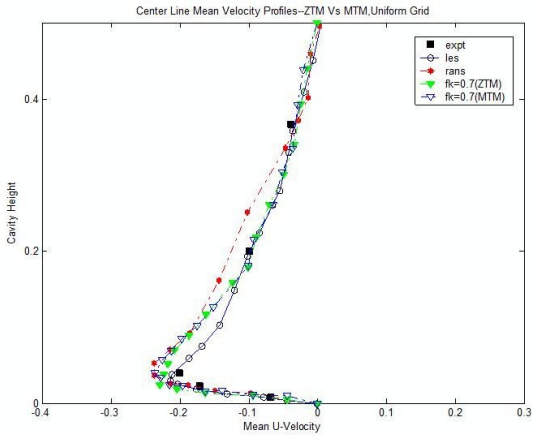

Figure 33. Cavity flow: RANS, LES and PANS (fk=0.2) comparison against experimental data.

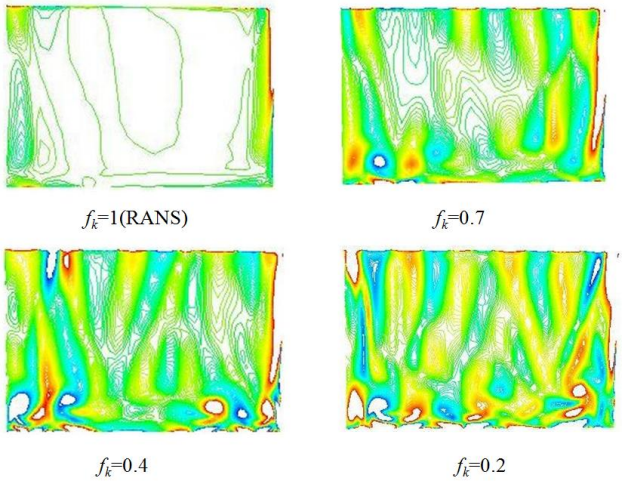

Figure 34. RANS and PANS vorticity contours

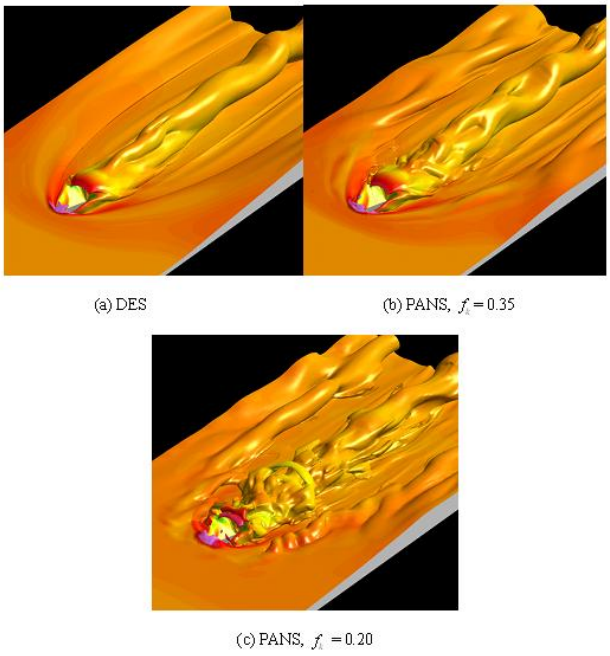

Figure 35. DES and PANS simulations of jet in cross-stream.

VI. Observations and Recommendations

We conclude in this section with some general observations followed by specific recommendations. The general remarks are:

- Increasing Mach number is generally coupled with decreasing Reynolds number. Such flows are perfect for DNS (or high-resolution LES).
- Canonical high Mach number experiments must be designed for DNS for mutual validation and enhancing knowledge of fundamental turbulence processes.
- All efforts must be made to perform experiment and DNS/LES at the same Reynolds number.
- We need to expand our interests to include: heat transfer, roughness, film cooling; ablation, wall catalysis, pyrolysis, real gas effects, chemistry; curvature, pressure gradient, three-dimensionality.
- Development of accurate high-speed high-enthalpy diagnostics are crucial for clearer understanding of the physics and closure modeling development and validation. New diagnostics for turbulent stresses, thermal fluxes, scalar fluxes and reaction processes are essential.

Hypersonic turbulence comprises of complex interactions between flow, thermodynamical and chemical processes. The governing parameter range is rich and it is important that we understand the various effects acting individually and collectively over a wide range of values. Some challenges and strategies for such a wide-ranging study are now identified.

- **Effects of Reynolds number:** At low Reynolds number, experiments should couple with DNS to allow direct comparison; At high Reynolds number, experiments should help improve LES and turbulence models
- *Effects of Mach number:* At low Mach number we need to deal with extensive regions of mixed subsonic and supersonic flow. At higher Mach number, true compressibility effects become apparent and Reynolds Analogy for turbulence may break down.
- **Heat transfer effects:** In equilibrium boundary layers, the velocity field is strongly coupled to the surface heat transfer, for the mean and fluctuating quantities (Reynolds analogies). In flows out of equilibrium, Reynolds analogies break down. In flows strongly out of equilibrium, the pressure field is strongly coupled to the surface heat transfer for the mean and fluctuating quantities.
- **Effects of curvature:** Boundary layer response depends on the sign of curvature, concave curvature is stabilizing and concave is destabilizing. At subsonic speeds the criteria for the appearance of Taylor-Gortler vortices are reasonably well understood. At supersonic speeds we have no clear guidance. The unsteady nature of Taylor-Gortler vortices in turbulent flow is not well understood.
- **Effects of pressure gradient:** In subsonic flows, the skin friction decreases with increasingly adverse pressure gradient. In supersonic flows, the skin friction increases with increasingly adverse pressure gradient. The skin friction (heat transfer) prediction depends strongly on the development of the velocity profile and the location of the sonic line.
- **Other effects:** Effects of impulsive changes in wall normal velocity, roughness, and heat transfer is not well known.
- **Three-dimensional interactions:** Single-sided interactions mimic fins and support problems, and are reasonably well understood (scaling, structure). Crossing shock interactions are found in inlets, and define downstream flow quality, mixing, and then combustion
- **Chemistry:** Almost no experiments exist that allow verification of non-equilibrium effects, real gas effects, catalysis, pyrolysis, ablation. There is even lesser turbulence data of such effects.

Some important lessons learned:

- Diagnostics are crucial to everything – understanding, modeling, validation, etc. Time- and space-resolved measurements are crucial. Identification of large-scale motions, so-called eddy chasing, is also important for understanding key turbulence mechanisms.
- Nevertheless, simple, well-chosen diagnostics can reveal important information for enhancing our undrerstanding of the turbulence processes.
- Validated DNS can be an effective investigative tool at low Reynolds number.
- In the hypersonic regime, apparently simple flows (e.g., slot injection) can turn out to be surprisingly complex.

Acknowledgments

The support of NASA under Cooperative Agreement No. NNX08AB46A (directed by Program Manager Catherine McGinley), No. NNX08AB44A (directed by Program Managers Aaron Auslender and Denis Yoder) is gratefully acknowledged, and NASA Cooperative Agreement No. NNX08AD0LA (directed by Peter Gnoffo), NASA CUIP Grant No. NCC3-989 (directed by Peter Gnoffo), AFOSR Grant # AF/9550-05-L0490 (directed by Joan Fuller), and AFOSR Grant # AF/9550-06-1-0323 (directed by John Schmisseur).

References

[1]Adams, N.A., Direct simulation of the turbulent boundary layer along a compression ramp at $M = 3$ and $Re_\theta = 1685$. Journal of Fluid Mechanics, **420**, pp. 47-83, 2000.

[2]Adumitroaie, V., Ristorcelli, J. R. and Taulbee, D. B., 1999. Progress in Favre-Reynolds stress closures for compressible flows. *Physics of Fluids*, **11**, pp. 2696–2719.

[3]Adrian, R., Meinhart, C., Tomkins, C., Vortex organization in the outer region of the turbulent boundary layer. J. Fluid Mech., **422**, pp. 1-54, 2000.

[4]Anderson, J. D., *Hypersonic and HIgh Temperature Gas Dynamics*. McGraw-Hill (1989).

[5]Auvity, B., Etz, M. R. and Smits, A. J. 2001. Effects of transverse helium injection on hypersonic boundary layers. *Physics of Fluids*, **13**, 10, 3025–3032.

[6]Balakumar, B.J., Adrian, R.J., Large- and very-large-scale motions in channel and boundary-layer flows. Phil. Trans. R. Soc. A, **365**, pp. 665-681, 2007.

[7]Baumgartner, M.L. 1997. *Turbulence Structure in a Hypersonic Boundary Layer*. Ph.D. Thesis, Princeton University.

[8]Beekman, Z., Priebe, S., Ringuette, M., and Martin Effect of Wall Temperature and Mach Number on the Turbulence Structure of Hypersonic Boundary Layers AIAA Paper No. 2009-1328, 2009

[9]Bookey, P., Wu, M., Smits, A. J. and Martin, P. 2005. New Experimental Data of STBLI at DNS/LES Accessible Reynolds Numbers, *AIAA Paper 2005-0309*.

[10]Bookey, P. Wyckham, C. M. and Smits A. J. 2005. Experimental Investigations of Mach 3 Shock-Wave Turbulent Boundary Layer Interactions, *AIAA Paper 2005-4899*.

[11]Brown, G.L., and Thomas, A.S.W. Large structure in a turbulent boundary layer. Phys. Fluids, **10** pp. 243-251, 1977.

[12]Cambon, C., Coleman, G. N. and Mansour, D. N. N. 1993. Rapid distortion analysis and direct simulation of compressible homogeneous turbulence at finite Mach number, *Journal of Fluid Mechanics*, **257**, pp. 641–665.

[13]Coleman, G. T. and Stollery, J. L. 1972. Heat transfer from hypersonic turbulent flow at a wedge compression corner. *Journal of Fluid Mechanics*, **56**, 741–752.

[14]Coles, D. 1962. The turbulent boundary layer in a compressible fluid. *Report R-403-PR, The Rand Corporation, Santa Monica, California*.

[15]Debiève, J.F., Dupont, P., Smith, D.R., and Smits, A.J. Supersonic turbulent boundary layer subjected to step changes in wall temperature AIAA Journal, **35** pp. 51-57, 1997

[16]del Álamo, J.C., and Jiménez, J. Spectra of the very large anisotropic scales in turbulent channels. journal = Phys. Fluids, **15** pp. L41–L44, 2003.

[17]del Álamo, J.C., Jiménez, J., Zandonade, P., and Moser, R.D. Scaling of the energy spectra of turbulent channels. J. Fluid Mech., **500** pp. 135–144, 2004.

[18]del Álamo, J.C., Jiménez, J., Zandonade, P., and Moser, R.D. Self-similar vortex clusters in the turbulent logarithmic region. J. Fluid Mech., **561** pp. 329–358, 2006.

[19]del Álamo, J.C., Jiménez, J., Zandonade, P., and Moser, R.D. Self-similar vortex clusters in the turbulent logarithmic region. J. Fluid Mech., **561** pp. 329-358, 2006

[20]Dussauge, J.-P. and Smits, A. J. 1995. Characteristic scales for energetic eddies in turbulent supersonic boundary layers. *In: Proceedings of the Tenth Symposium on Turbulent Shear Flows*. Pennsylvania State University.

[21]Dussauge, J. P. and Dupont, P. and Debiève, J. F. Unsteadiness in Shock Wave Boundary Layer Interactions with Separation journal = Aerospace Science and Technology, **10** 2006

[22]Eléna, M., J.P. Lacharme, and J. Gaviglio title = Comparison of hot-wire and laser doppler anemometry methods in supersonic turbulent boundary layers In: Dybb, A. & Pfund, P.A. (eds), International Symposium on Laser Anemometry. ASME, 1985

[23]Eléna, M. and J.P. Lacharme Experimental Study of a supersonic turbulent boundary layer using a laser Doppler anemometer Journal Mécanique THéorique et Appliquée, **7**, pp. 175–190, 1988

[24]D.A. Johnson and W.C. Rose Laser velocimetry and hot-wire anemometer comparison in a supersonic boundary layer AIAA Journal, **13**, pp. 512–515, 1975

[25]Duan, L., and Martin, M.P. Effect of Finite-rate Chemical Reactions on Turbulence in Hypersonic Turbulent Boundary-Layers AIAA Paper No. 2009-588, 2009

[26]Elfstrom, G. M. 1972. Turbulent hypersonic flow at a wedge compression corner. *Journal of Fluid Mechanics*, **53**, 113–127, 1972.

[27]Evans, T. and Smits, A.J. 1996. Measurements of the Mean Heat Transfer in a Shock Wave Turbulent Boundary Layer Interaction. *Experimental Thermal and Fluid Science*, **12**(1), 87–97.

[28]Fernholz, H.H. and Finley, P.J. 1976. A critical compilation of compressible turbulent boundary layer data. *AGARDograph 223*.

[29]Fernholz, H.H. and Finley, P.J. 1980. A critical commentary on mean flow data for two-dimensional compressible turbulent boundary layers. *AGARDograph 253*.

[30]Fernholz, H.H. and Finley, P.J. 1981. A further compilation of compressible turbulent boundary layer data with a survey of turbulence data. *AGARDograph 263*.

[31]Fernholz, H.H., Smits, A.J., Dussauge, J.P. and Finley, P.J. 1989. A survey of measurements and measuring techniques in rapidly distorted compressible turbulent boundary layers. *AGARDograph 315*.

[32]Flores, O, J. Jiménez and J. C. del Álamo Vorticity organization in the outer layer of turbulent channels with disturbed walls J. Fluid Mech., **591**, pp. 145–154, 2007

[33]Ganapathisubramani, B., E. K. Longmire and I. Marusic Characteristics of vortex packets in turbulent boundary layers journal = J. Fluid Mech., **478**, pp. 35–46, 2003

[34]Ganapathisubramani, B., N. Clemens and D. Dolling Large-scale motions in a supersonic turbulent boundary layer J. Fluid Mech., **556**, pp. 1–11, 2006.

[35]Ganapathisubramani, B., N. Clemens and D. Dolling Effects of upstream boundary layer on the unsteadiness of shock-induced separation J. Fluid Mech., **585**, pp. 369–394, 2007

[36]Garg, S. and Settles, G.S. 1993. Wall pressure fluctuations beneath swept shock/boundary layer interactions. *AIAA Paper 93-0384*.

[37]Girimaji, S. S. 1996 Fully explicit and self-consistent algebraic Reynolds stress model *Theoretical and Computational Fluid Dynamics*, **8**(6), 387–402.

[38]Girimaji, S. S. 1997. A Galilean invariant explicit algebraic Reynolds stress model for turbulent curved flows *Physics of Fluids*, **9**(4), 1067–1077.

[39]Girimaji, S. S. 2000. Pressure-strain correlation modelling of complex turbulent flows. *Journal of Fluid Mechanics*, **422**, 91–123.

[40]Girimaji, S. S. 2001. Lower-dimensional manifold (algebraic) representation of Reynolds stress closure equations *Theoretical and Computational Fluid Dynamics*, **14**(4), 259—281.

[41]Girimaji, S. S., Jeong, E., Poroseva S.V. 2003. Pressure-strain correlation in homogeneous anisotropic turbulence subject to rapid strain-dominated distortion *Physics of Fluids*, **15**(10), 3209–3222.

[42]Girimaji S. S. 2004. A new perspective on realizability of turbulence models *Journal of Fluid Mechanics*, **512**, 191–210.

[43]Girimaji, S. S. 2006. Partially-averaged Navier-Stokes model for turbulence: A Reynolds-averaged Navier-Stokes to direct numerical simulation bridging method *Journal of Applied Mechanics-Transactions of the ASME*, **73**(3), 413–421.

[44]Girimaji, S. S., Jeong, E. and Srinivasan, R. 2006. Partially averaged Navier-Stokes method for turbulence: Fixed point analysis and comparison with unsteady partially averaged Navier-Stokes *Journal of Applied Mechanics-Transactions of the ASME*, **73**(3), 422–429.

[45]Grube, N. and P. Martin Assessment of Subgrid- Scale Models and Shock- Confining Filters in Large- Eddy Simulation of Highly Compressible Isotropic Turbulence AIAA-2009-947

[46]Guala, M. S. E. Hommema and R. J. Adrian Large-scale and very-large-scale motions in turbulent pipe flow. J. Fluid Mech., **554** pp. 521–542, 2006

[47]Guarini, S.E., R.D. Moser, K. Shariff and A. Wray Direct numerical simulation of supersonic turbulent boundary layer at Mach 2.5 Journal of Fluid Mechanics, **414**, pp. 1–3, 2000

[48]Hambleton, W.T., N. Hutchins and I. Marusic Simultaneous orthogonal-plane particle image velocimetry measurements in a turbulentboundary layer J. Fluid Mech., **560** pp. 53–64, 2006

[49]Head, M. and P. Bandyopadhyay New aspects of turbulent boundary-layer structure J. Fluid Mech., **107**, pp. 297–338, 1981

[50]Hutchins, N., and I. Marusic Investigation of the log region structure in wall bounded turbulence AIAA Paper 2006-325, 2006

[51]Hutchins, N., and I. Marusic Evidence of very long meandering features in the logarithmic region of turbulent boundary layers J. of Fluid Mechanics, **579**, pp. 1-28, 2007

[52]Hutchins, N., and I. Marusic Large-scale influences in near-wall turbulence Phil. Trans. R. Soc. A, **365** pp. 647–664, 2007

[53]Jaberi, F.A., D. Livescu and C.K. Madnia Charateristics of chemically reacting compressible homogeneous turbulence Physics of Fluids, **12**, pp. 1189–1209, 2000

[54]Jiménez, J. The largest scales of turbulent wall flows Center for Turbulence Research, Annual Research Briefs, Stanford University, 137–154, 1998

[55]Kim, H., S. Kline and W. Reynolds The production of turbulence near a smooth wall in a turbulent boundary layer J. Fluid Mech., **50**, pp. 133-160, 1971

[56]Kim, K.C., and R. J. Adrian Very large-scale motion in the outer layer Phys. Fluids, **11** pp. 417–422, 1999

[57]Klebanoff, P.S. Characteristics of turbulence in a boundary layer with zero pressure gradient NACA Report 1247, 1955

[58]Kimmel, R. L. 1993. Experimental transition zone lengths in pressure gradient in hypersonic flow. In: Kral L. D., Zang T. A., editors. Transitional and turbulent compressible flows *FED* **151**. New York: ASME, 117–27.

[59]Kimmel, R. L. 1997. The effects of pressure gradients on transition zone length in hypersonic boundary layers. *J. Fluids Eng.*, **119**(1) 36–41.

[60]Konrad, W. 1993. *A three-dimensional supersonic turbulent boundary layer generated by an isentropic compression.* Ph.D. Thesis, Princeton University, Princeton, NJ.

[61]Lakshmipathy, S., Girimaji, S. S. 2007 Extension of Boussinesq turbulence constitutive relation for bridging methods *Journal of Turbulence*, **8**(31), 1–21.

[62]T. A. Lavin, *Reynolds and Favre-averaged rapid distortion theory for compressible, ideal-gas turbulence*, MSE Thesis. Texas A&M University (2007).

[63]Lee, K., Girimaji S. S. and Kerimo, J. 2008. Validity of Taylor's dissipation-viscosity independence postulate in variable-viscosity turbulent fluid mixtures *Physical Review Letters*, **101**(7).

[64]Martin, M.P. and G.V. Candler Effect of Chemical Reactions on Decaying Isotropic Turbulence Physics of Fluids, **10** pp. 1715-1724, 1998

[65]Martin, M.P. and G.V. Candler Subgrid-Scale Model for the Temperature Fluctuations in Reacting Hypersonic Turbulent Flows Physics of Fluids, bf 11 pp. 27652771, 1999

[66]Martin, M.P. and G.V. Candler DNS of Mach 4 boundary layer with chemical reactions AIAA Paper No.2000-0399, 2000

[67]Martin, M.P. and G.V. Candler Temperature Fluctuation Scaling in Reacting Turbulent Boundary Layers AIAA Paper No.01-2717, 2001

[68]Martin, M.P. Exploratory Studies of Turbulence/Chemistry Interation in Hypersonic Flows AIAA Paper No. 03-4055, 2003

[69]Martin, M.P. 2004. DNS of hypersonic turbulent boundary layers. *AIAA Paper 2004-2337*.

[70]Martin, M.P. Direct numerical simulation of hypersonic turbulent boundary layers. Part 1: initialization and comparison with experiments J. Fluid Mech., **570** pp. 347–364, 2007

[71]Martin, M.P., and Candler, G.V. Temperature Fluctuation Scaling in Reacting Boundary Layers AIAA Paper No. 2001-2717

[72]Marusic, I, and N. Hutchins Experimental study of wall turbulence: Implications for control Transition and Turbulence Control, Gad-el-Hak, M., 2005

[73]McGinley, C.B., Spina, E.F. and Sheplak, M. Turbulence measurements in a Mach 11 helium turbulent boundary layer. *AIAA Paper 94-2364*.

[74]Mikulla, V. and Horstman, C. C. 1976. Turbulence measurements in hypersonic shock-wave boundary-layer interaction flows. *AIAA Journal*, **14**(5) 568–575.

[75]Modest, M., Levin, D., and Martin, M.P. Progress on turbulence-radiation interaction Annual Report on CUIP NASA Grant # NCC3-989, presentation to Peter Gnoffo, Jan., 2009

[76]O'Farrell, C. and M.P. Martin Chasing Eddies and Their Wall Signature in DNS Data of Turbulent Boundary Layers submitted to Journal of Turbulence 2009

[77]Owen, F. K. and Horstman, C. C. 1972. On the structure of hypersonic turbulent boundary layers. *Journal of Fluid Mechanics*, **53** 611–636.

[78]Owen, F. K. and Horstman, C. C. 1972. Turbulent properties of a compressible boundary layer. *AIAA Journal*, **10**(1) 1418–1424.

[79]Owen, F. K., Horstman, C. C. and Kussoy, M. I. 1975. Mean and fluctuating flow measurements on a fully-developed non-adiabatic hypersonic boundary layer. *Journal of Fluid Mechanics*, **70** 393–413.

[80]Pirozzoli, S., F. Grasso and T.B. Gatski Direct numerical simulation and analysis of a spatially evolving supersonic turbulent boundary layer at M=2.25 Phys. Fluids, **16** pp. 530–545, 2004.

[81]Pirozzoli, S. and F. Grasso Direct numerical simulation of impinging shock wave/turbulent boundary layer interaction at M=2.25 Phys. Fluids, **18**, 2006

[82]Poggie, J. 1995. *On the control of a compressible, reattaching shear layer.* Ph.D. Thesis, Princeton University.

[83]Poggie, J., Smits, A.J. and Glezer, A. 1992. The dynamics and control of fluctuating pressure loads in the reattachment region of a supersonic free shear layer. *AIAA Paper 92-0178*.

[84]Priebe, S., Wu, M., and Martin, M.P. Direct Numerical Simulation of Shockwave and Turbulent Boundary Layer Interactions AIAA Paper No. 2009-589, 2009

[85]Ringuette, M. J., Martin, M. P. and Smits, A. J. 2006. Characterization of the turbulence structure in supersonic boundary layers using DNS data. *AIAA Paper 2006-3539*.

[86]Ringuette, M. J. and Smits, A. J. 2007. Wall-pressure measurements in a Mach 3 shock-wave turbulent boundary layer interaction at a DNS accessible Reynolds number. *AIAA Paper 2007-4113*.

[87]Ringuette, M.J., M. Wu and M. P. Martín Coherent structures in direct numerical simulation of turbulent boundary layers at Mach 3 J. Fluid Mech., **594** pp. 59–69, 2008a

[88]Ringuette, M.J., M. Wu and M. P. Martín Low Reynolds Number Effects in a Mach 3 Shock Turbulent Boundary Layer Interaction AIAAJ., **46** pp. 1884–1887, 2008b

[89]Ringuette, M.J., P. Bookey, C. Wyckham, A. J. Smits Experimental study of a Mach 3 compression ramp interaction at $\Re_\theta = 2400$. AIAA Journal, to appear

[90]S.K. Robinson and M.L. Seegmiller and M.I. Kussoy Hot-wire and laser Doppler anemometer measurements in a supersonic boundary layer AIAA Paper No. 83-1723, 1983

[91]Roy, C. J. and Blottner, F. G. Review and assessment of turbulence models for hypersonic flows. *Progress in Aerospace Sciences*, **42**, 469–530, 2006.

[92]Rubinstein, R. and Girimaji S.S., 2006 Second moment closure near the two-component limit *Journal of Fluid Mechanics*, **548**, 197–206.

[93]Sahoo, D., Ringuette, M. J. and Smits, A. J. 2009. Experimental investigation of hypersonic turbulent boundary layers. *AIAA Paper 2009-0780*.

[94]Sambasivam, A., Girimaji S. S. and Poroseva S. V. 2004. Realizability of the Reynolds stress and rapid pressure-strain correlation in turbulence modelling *Journal of Turbulence*, **5**(006).

[95]S. Sarkar, The stabilizing effect of compressibility in turbulent shear flow, *Journal of Fluid Mechanics*, **282**, (1995) pp 163–186.

[96]Selig, M.S., Andreopoulos, J., Muck, K.C., J.P. Dussauge and Smits, A.J., Turbulence Structure in a Shock-Wave/Turbulent Boundary Layer Interaction, *AIAA Journal*, **27**, 862–869, 1989.

[97]Settles, G.S. and Teng, H.Y. 1984. Cylindrical and conical upstream influence regimes of three-dimensional shock/turbulent boundary layer interactions. *AIAA Journal*, **22**, 194–200.

[98]Settles, G.S. and Dodson, L.J. 1991. Hypersonic shock-boundary layer interaction database. *NASA CR 177577*.

[99]Shen, Z.H., Smith, D.R. and Smits, A.J. 1993. Wall pressure fluctuations in the reattachment region of a supersonic free shear layer. *Experiments in Fluids*, **14**, 10–16.

[100]Smith, D.R., Poggie, J., Konrad, W. and Smits, A.J. 1991. Visualization of the structure of shock wave turbulent boundary layer interactions using Rayleigh scattering. *AIAA Paper 91-0651*.

[101]Smits, A.J. and Wood, D.H. 1987. Experimental study of three shock wave turbulent boundary-layer interactions. Annual Review of Fluid Mechanics, **17**, 321–358, 1985.

[102]Smits, A.J. and Muck, K.C. 1987. Experimental study of three shock wave turbulent boundary-Layer interactions. Journal of Fluid Mechanics, **182**, 291–314, 1987.

[103]Smits, A.J., E.F. Spina, A.E. Alving, R.W. Smith, E.M. Fernando, J.F. Donovan A comparison of the turbulence structure of subsonic and supersonic boundary layers Phys. Fluids A, **1** pp. 1865–1875, 1989

[104]Smits A. J. and Dussauge J.-P. 2005 *Turbulent Shear Layers In Supersonic Flow*. Springer-Verlag New York Inc., 2005.

[105]Spina, E.F. Donovan, J.F., and Smits, A.J. 1991. On the structure of high-Reynolds-number supersonic turbulent boundary layers. Journal of Fluid Mechanics, **222**, 293–327.

[106]Spina, E.F., Smits, A.J. and Robinson, S.K. 1994. The physics of supersonic turbulent boundary layers. Annual Review of Fluid Mechanics, **26**, 287–319, 1994.

Tan, D.K.M., Tran, T.T. and Bogdonoff, S.M. 1985. Surface pressure fluctuations in a three-dimensional shock wave/turbulent boundary layer interaction. *AIAA Paper 85-0125*.

[107]E. M. Taylor and N. Grube and M. P. Martín Evaluation of traditional and shock-confininf LES filters using data of compressible turbulence AIAA Paper Number 2007-4197

[108]E. M. Taylor and M. P. Martín Direct Numerical Simulations of Compressible Isotropic Turbulence Interacting with Shock Waves Under consideration for publication in Physics of Fluids, 2009

[109]Theodorsen, T. Mechanism of Turbulence Proc. 2nd. Midwestern Conf. on Fluid Mech., pp. 1–19, Ohio State University, Columbus, Ohio, USA. 1952.

[110]Thomas, A.S.W., and M. K. Bull On the role of wall-pressure fluctuations in deterministic motions in the turbulent boundary layer J. Fluid Mech., **128**, pp. 283–322, 1983

[111]Tomkins, C. and R. Adrian Spanwise structure and scale growth in turbulent boundary layers J. Fluid Mech., **490** pp. 37-74, 2003

[112]Tran, T.T. 1987. *An experimental investigation of unsteadiness in swept shock wave/turbulent boundary layer interactions*. Ph.D. Thesis, Princeton University.

[113]Schrijer, F.F.J., F. Scarano and B.W. van Oudheusden Application of PIV in a Mach 7 double-ramp flow, Experiments in Fluids, **41**, pp. 353–363, 2006

[114]van Oudheusden, B.W. Principles and application of velocimetry-based planar pressure imaging in compressible flows with shocks Experiments in Fluids (electronic Open Access), 2008

[115]Humble, R.A., F. Scarano and B.W. van Oudheusden Experimental study of an incident shock wave/turbulent boundary layer interaction using PIV AIAA Paper Number 2006-3361, 2006

[116]Watson, R. D., Harris, J. D. and Anders, J. B. 1973. Measurements in a transitional/turbulent Mach 10 boundary layer at high Reynolds number. *AIAA Paper 73-165*.

[117]Wu, M., and Martin, M.P. 2007. Direct numerical simulation of shockwave and turbulent boundary layer interaction induced by a compression ramp. AIAA Journal, **45**, 879–889, 2007.

[118]Wu, M and M.P. Martín Analysis of shock motion in shockwave and turbulent boundary layer interaction usingdirect numerical simulation data J. of Fluid Mechanics, **594**, pp. 71–83, 2008

[119]

[120]Zhong, F., and Brown, G.L. 2005. Experimental and numerical studies of multi-hole cooled ceramic composite liners. *AIAA Paper 2005-0184*.

[121]Zhong, F., and Brown, G.L. 2006. A three-dimensional, coupled, heat transfer model for multi-hole cooling and comparisons with experiments. *AIAA Paper 2006-0595*.

[122]Zhou, J., R. Adrian, S. Balachandar ,and T. Kendall Mechanisms for generating coherent packets of hairpin vortices in channel flow J. Fluid Mech., **387**, pp. 353–396, 1999